Journal of Computational Physics xxx (2012) xxx–xxx

Contents lists available at SciVerse ScienceDirect

Journal of Computational Physics

journal homepage: www.elsevier.com/locate/jcp

Numerical methods for the simulation of a corrosion model with moving oxide layer ☆

C. Bataillon [a], F. Bouchon [b,c], C. Chainais-Hillairet [d,e,1], J. Fuhrmann [f,*], E. Hoarau [g], R. Touzani [b,c]

[a] CEA, DEN, DANS, DPC, SCCME, LECA, F-91191 Gif sur Yvette Cedex, France
[b] Université Blaise Pascal, Laboratoire de Mathématiques, BP10448, F-63000 Clermont-Ferrand, France
[c] CNRS, UMR 6620, Laboratoire de Mathématiques, F-63177 Aubière, France
[d] Laboratoire P. Painlevé, CNRS UMR 8524, Université Lille 1, 59655 Villeneuve d'Ascq Cedex, France
[e] Project-team SIMPAF, INRIA Lille-Nord-Europe, 59650 Villeneuve d'Ascq, France
[f] Weierstrass Institute for Applied Analysis and Stochastics, Mohrenstrasse 39, 10117 Berlin, Germany
[g] ANDRA/DS, 92298 Châtenay-Malabry Cedex, France

ARTICLE INFO

Article history:
Received 11 April 2011
Received in revised form 31 May 2012
Accepted 5 June 2012
Available online xxxx

Keywords:
Corrosion modeling
Drift–diffusion system
Moving boundaries
Adaptive time stepping

ABSTRACT

In this paper, we design numerical methods for a PDE system arising in corrosion modeling. This system describes the evolution of a dense oxide layer. It is based on a drift–diffusion system and includes moving boundary equations. The choice of the numerical methods is justified by a stability analysis and by the study of their numerical performance. Finally, numerical experiments with real-life data shows the efficiency of the developed methods.

1. Introduction

1.1. General framework of the study

The concept for long term storage of high-level radioactive waste in France under study is based on an underground repository. The waste shall be confined in a glass matrix and then placed into cylindrical steel canisters. These containers shall be placed into micro-tunnels in the highly impermeable Callovo-Oxfordian claystone layer at a depth of several hundred meters. At the request of the French nuclear waste management agency ANDRA, investigations are conducted to optimize and finalize this repository concept with the aim to ensure its long-term safety and its reversibility. In particular, the repository concept requires a minimum containment time of 1000 years.

The long-term safety assessment of the geological repository has to take into account the degradation of the carbon steel used for the waste overpacks and the cell disposal liners, which are in contact with the claystone formation. This degradation is mainly caused by generalized corrosion processes which form a passive layer on the metal surface consisting of a dense

☆ This work has been supported by the Nuclear Waste Management Agency ANDRA.
* Corresponding author. Tel.: +49 30 20372 560; fax: +49 30 2044975.
E-mail addresses: Christian.Bataillon@cea.fr (C. Bataillon), Francois.Bouchon@math.univ-bpclermont.fr (F. Bouchon), Claire.Chainais@math.univ-lille1.fr (C. Chainais-Hillairet), juergen.fuhrmann@wias-berlin.de (J. Fuhrmann).
[1] Partially supported from the ANR VFSitCom and from the GDR MOMAS CNRS/PACEN.

0021-9991/$ - see front matter © 2012 Elsevier Inc. All rights reserved.
http://dx.doi.org/10.1016/j.jcp.2012.06.005

oxide inner layer and a porous hydroxide outer layer in contact with the groundwater in the pore space of the claystones. The processes take place under anaerobic conditions, since the groundwater is anoxic.

The neighboring geochemical environment (pH, concentrations) and groundwater flow trends induce changes of the corrosion conditions, which, in turn, influence the geochemical and thermo-hydro-mechanics of the claystones. The temperature also affects the corrosion conditions. Indeed, the waste canisters are a source of heat. At the beginning of the repository development, the temperature is estimated to be about 90 °C. Later, it is supposed to reach its steady-state value near 40 °C.

As a tool to investigate the corrosion processes at the surface of the carbon steel canisters, the Diffusion Poisson Coupled Model (DPCM) for corrosion has been developed by Bataillon et al. [1].

The model focuses on the development of the dense oxide layer in the region of contact between the claystones and the metal. In order to reduce complexity, in the present paper, the porous hydroxide layer is not taken into account. The system claystones – oxide layer – metal is described by a coupled system of electromigration – diffusion equations for the transport of the charge carriers in the oxide layer, and a Poisson equation for the electric potential. The interaction between the oxide layer and the adjacent structures are described in terms of Robin boundary conditions for the electrochemical reactions and the potential drops. The system includes moving boundary equations based on the Pilling–Bedworth ratio. The system evolution can be investigated in both potentiostatic and galvanostatic situations. As the oxide layer is very thin compared to the waste overpack size, it is sufficient to consider the model in one space dimension.

The model allows to assess the evolution of the carbon steel corrosion rate, the chemical species release and the characteristic time of these processes. These data shall be used to estimate the lifetime of the carbon steel overpack and the pressure rise resulting from hydrogen release.

Carbon steel is expected to exhibit a corrosion rate between 1 and 10 μm year^{-1}. Due to the formation of the oxide layer, we expect a reduction of the corrosion rate.

1.2. Presentation of the corrosion model

We recall here the DPCM model introduced by Bataillon et al. [1]. The domain under study is the oxide layer whose interfaces are moving. The moving domain is denoted by $(X_0(t),X_1(t))$. In the oxide layer, three charge carriers are taken into account: electrons, cations (Fe^{3+}) and oxygen vacancies ($V_{\ddot{O}}$). The densities of these charge carriers are respectively denoted by N, P and C. The corresponding current densities are denoted by J_N, J_P and J_C. These current densities contain a drift part and a diffusion part, so that the equations for N, P and C are linear convection–diffusion equations. They are coupled with a Poisson equation for the electrical potential Ψ.

Charge carriers are created and consumed at both interfaces: $x = X_0(t)$ is the outer interface (oxide/solution) and $x = X_1(t)$ is the inner interface (oxide/metal). The kinetics of the electrochemical reactions at interfaces leads to Robin boundary conditions on N, P and C.

The boundary conditions for the Poisson equation take into account that the metal and the solution can be charged because they are respectively electronic and ionic conductors. Such an accumulation of charges induces a field given by the Gauss law. These accumulations of charges depend on the voltage drop at the interface by the usual Helmholtz law which links the charge to the voltage drop through a capacitance. The parameters $\Delta\Psi_1^{pzc}$ and $\Delta\Psi_0^{pzc}$ are the voltage drop corresponding to no accumulation of charges respectively in the metal and in the solution.

The DPCM model takes into account the growth of the oxide host lattice at $x = X_1(t)$ and its dissolution at $x = X_0(t)$ leading to moving boundary equations. In order to properly reflect the mass balance an the moving interfaces, in the boundary conditions, we need to take into account the interface velocities. This is a consequence, e.g., of the pillbox lemma [2,3]. The dimensionless model writes for $t \geqslant 0$:

- Equation and boundary conditions for the density of cations P:

$$\partial_t P + \partial_x J_P = 0, \quad J_P = -\partial_x P - 3P\partial_x \Psi, \quad x \in (X_0(t), X_1(t)), \tag{1.1a}$$

$$J_P + PX_0'(t) = m_P^0 (P^m - P) e^{-3b_P^0 \Psi} - k_P^0 P e^{3a_P^0 \Psi}, \quad x = X_0(t), \tag{1.1b}$$

$$J_P + PX_1'(t) = m_P^1 P e^{-3b_P^1 (V-\Psi)} - k_P^1 (P^m - P) e^{3a_P^1 (V-\Psi)}, \quad x = X_1(t). \tag{1.1c}$$

- Equation and boundary conditions for the density of electrons N:

$$\frac{D_1}{D_2} \partial_t N + \partial_x J_N = 0, \quad J_N = -\partial_x N + N\partial_x \Psi, \quad x \in (X_0(t), X_1(t)), \tag{1.2a}$$

$$J_N + NX_0'(t) = m_N^0 e^{b_N^0 \Psi} - k_N^0 N e^{-a_N^0 \Psi} + n_N^0 e^{a_r^0 \Psi} - p_N^0 N e^{-b_r^0 \Psi}, \quad x = X_0(t), \tag{1.2b}$$

$$J_N + NX_1'(t) = m_N^1 N - k_N^1 N_{metal} \log(1 + e^{-(V-\Psi)}), \quad x = X_1(t). \tag{1.2c}$$

- Equation and boundary conditions for the density of oxygen vacancies C:

$$\frac{D_1}{D_3} \partial_t C + \partial_x J_C = 0, \quad J_C = -\partial_x C - 2C\partial_x \Psi, \quad x \in (X_0(t), X_1(t)), \tag{1.3a}$$

$$J_C + CX_0'(t) = m_C^0\left(1-\frac{C}{4}\right)e^{-2b_C^0\Psi} - k_C^0\frac{C}{4}e^{2a_C^0\Psi}, \quad x = X_0(t), \tag{1.3b}$$

$$J_C + CX_1'(t) = m_C^1\frac{C}{4}e^{-3b_C^1(V-\Psi)} - k_C^1\left(1-\frac{C}{4}\right)e^{3a_C^1(V-\Psi)} \quad x = X_1(t). \tag{1.3c}$$

- Equation on the electrical potential Ψ:

$$-\lambda^2\partial_{xx}^2\Psi = 3P - N + 2C + \rho_{hl}, \quad x \in (X_0(t), X_1(t)), \tag{1.4a}$$

$$\Psi - \alpha_0\partial_x\Psi = \Delta\Psi_0^{pzc}, \quad x = X_0(t), \tag{1.4b}$$

$$\Psi + \alpha_1\partial_x\Psi = V - \Delta\Psi_1^{pzc}, \quad x = X_1(t). \tag{1.4c}$$

- Moving boundary equations

$$\frac{dX_0}{dt} = v_d^0(t) + \frac{dX_1}{dt}\left(1 - \frac{\Omega_{ox}}{m\Omega_{Fe}}\right), \tag{1.5a}$$

$$\frac{dX_1}{dt} = -\frac{D_3}{4D_1}\frac{\Omega_{Fe}}{\Omega_{ox}}\left(J_C(X_1) + CX_1'(t)\right), \tag{1.5b}$$

$$\text{with } v_d^0(t) = k_d^0 e^{-5a_d^0\Psi(X_0(t))}. \tag{1.5c}$$

The system is supplemented with initial conditions:

$$N(x,0) = N^0(x), \quad P(x,0) = P^0(x), \quad C(x,0) = C^0(x), \quad x \in (0,1), \tag{1.6a}$$

$$X_0(0) = 0, \quad X_1(0) = 1. \tag{1.6b}$$

We shortly explain the parameters of the model:

- D_1, D_2 and D_3 are respectively the mobility or diffusion coefficients of cations, electrons and oxygen vacancies. D_1 and D_3 have the same order of magnitude, but $D_1 \ll D_2$ due to the difference of size between cations and electrons and the resulting difference of mobilities.
- $\left(m_P^i, k_P^i\right)_{i=0,1}$, $\left(m_N^i, k_N^i\right)_{i=0,1}$, $\left(m_C^i, k_C^i\right)_{i=0,1}$, (n_N^0, p_N^0), k_d^0 are interface kinetic functions. We assume that these functions are constant and strictly positive.
- $\left(a_u^0, b_u^0\right)$ for $u = P,N,C,r,d$ and $\left(a_u^1, b_u^1\right)$ for $u = P,C$ are positive transfer coefficients.
- P^m is the maximum occupancy for octahedral cations in the host lattice.
- N_{metal} is the electron density of state in the metal (Friedel model).
- ρ_{hl} is the net charge density of the ionic species in the host lattice. We assume that ρ_{hl} is homogeneous.
- Ω_{ox} is the molar volume of the oxide.
- Ω_{Fe} is the molar volume of the metal.
- m is the number of moles of iron per mole of oxide ($m = 3$ for magnetite).
- $\Delta\Psi_0^{pzc}$, $\Delta\Psi_1^{pzc}$ are respectively the outer and the inner voltages of zero charge.
- λ^2, α_0, α_1 are positive dimensionless parameters.

In the system (1.1)–(1.5), V can either be considered as an applied potential (“potentiostatic case”) or be given by another equation ensuring the electron charge balance at the inner interface (“galvanostatic case”):

$$-3\left(J_P + PX_1'(t) + \frac{D_3}{4D_1}\left(J_C + CX_1'(t)\right)\right) + \frac{D_2}{D_1}\left(J_N + NX_1'(t)\right) = \widetilde{J}, \ x = X_1(t) \tag{1.7}$$

If $\widetilde{J} = 0$, we speak of free corrosion, in this case, V is called “free corrosion potential”.

Remark 1.1. The equations for the carrier densities with their boundary conditions (1.1)–(1.3) have the same form. They can all be written:

$$\varepsilon_u\partial_t u + \partial_x J_u = 0, \quad J_u = -\partial_x u - z_u u\partial_x\Psi \text{ in } (X_0(t), X_1(t)), \quad \forall t \geqslant 0, \tag{1.8a}$$

$$-J_u - uX_0'(t) = r_u^0(u(X_0(t)), \Psi(X_0(t))) \text{ on } x = X_0(t), \quad \forall t \geqslant 0, \tag{1.8b}$$

$$J_u + uX_1'(t) = r_u^1(u(X_1(t)), \Psi(X_1(t)), V) \text{ on } x = X_1(t), \quad \forall t \geqslant 0. \tag{1.8c}$$

For $u = P,N,C$, the charge numbers of the carriers are respectively $z_u = 3, -1, 2$ and we respectively have $\varepsilon_u = 1, \frac{D_1}{D_2}, \frac{D_1}{D_3}$. We also note that both functions r_u^0 and r_u^1 are linear and monotonically increasing with respect to their first argument. More precisely, the functions r_u^0 and r_u^1 have the following form:

Please cite this article in press as: C. Bataillon et al., Numerical methods for the simulation of a corrosion model with moving oxide layer, J. Comput. Phys. (2012), http://dx.doi.org/10.1016/j.jcp.2012.06.005

$$r_u^0(s,x) = \beta_u^0(x)s - \gamma_u^0(x), \tag{1.9a}$$

$$r_u^1(s,x,V) = \beta_u^1(V-x)s - \gamma_u^1(V-x), \tag{1.9b}$$

where $\beta_u^0, \beta_u^1, \gamma_u^0, \gamma_u^1$ are smooth positive functions.

1.3. Main results

The system of equations (1.1a)–(1.4a) is close to the van Roosbroeck's drift–diffusion system arising in semiconductor modeling (with three charge carriers instead of two). In the semiconductor framework, the drift–diffusion system is defined on a fixed domain and is usually supplemented with Dirichlet, Neumann or Robin boundary conditions. Furthermore, an additional coupling is given by reaction terms in the interior of the domain which describe the generation and recombination of the charge carriers. It has been shown that the van Roosbroek system exhibits global existence and uniqueness results under natural assumptions (see [4–8]). Existence results for the case of more than two species motivated by dopant diffusion in semiconductors can be found in [9].

In the present paper, no reactions take place in the interior of the domain, and the boundary conditions supplementing the drift–diffusion equations are given by Butler–Volmer-like laws at the interfaces. They lead to nonlinear Robin boundary conditions which induce an additional coupling in the system. Moreover, the system includes equations for the position of the moving boundary. Theoretical results (existence, uniqueness, long-time behavior) for (1.1)–(1.7) have not been proven yet. These questions can possibly be studied by combining the techniques developed in the semiconductor framework cited above and ideas by Aiki, Böhm and Muntean [10,3,11,12] for somewhat simpler systems with one moving interface.

While these questions are worth to be studied, due to the significant interest in the ability to use this model in simulations within the framework described in the introduction, the aim of the present paper is rather the numerical approximation of the corrosion model. We want to propose an efficient numerical method in order to solve the full DPCM model (1.1)–(1.7).

In Section 2 we focus on the discretization of the system of convection–diffusion equations coupled with the Poisson equation (1.1)–(1.4). Therefore, we study a simplified two-species model on a fixed domain discretized by the finite volume method and study two different choices for the time discretization. The stability analysis of both schemes will show that a fully implicit time discretization must be chosen.

Then, in Section 3, we consider the full system in the potentiostatic case with the moving boundary equations. We introduce a change of variables in order to rewrite the system on a fixed domain and adapt the scheme designed in Section 2. We will study two different possibilities for the time discretization of the interface equations. We will also consider the galvanostatic case by taking into account Eq. (1.7).

In Section 4, we will give some details on the practical implementation of the numerical methods proposed in Section 3. Some improvements, like adaptive time stepping, will also be proposed. The performance of the designed numerical methods will be studied in Section 5. Finally, Section 6 is devoted to the presentation of some numerical experiments in a real-life context.

2. Study of a simplified model, choice for the time discretization

In this Section, we focus on a two-species model in order to fix the choice of the time discretization for our scheme. We just consider the case with electrons and cations Fe^{3+}. Without oxygen vacancies, there will be no evolution of the oxide layer: the domain will be considered as fixed. Furthermore, we consider here the potentiostatic case: V is an applied potential.

2.1. Presentation of the simplified model and discretization

The simplified system is obtained from (1.1), (1.2), (1.4) by setting $C = 0$ and $X_0(t) = 0$, $X_1(t) = 1$ for all t. It consists of two drift–diffusion equations for the charge densities, coupled with a Poisson equation for the electrostatic potential. The boundary conditions are Robin boundary conditions.

For the sake of simplicity, we also assume that the boundary conditions on P and N have exactly the same form. It means that the functions β_u^0, γ_u^0, β_u^1 and γ_u^1 defined in (1.9a) and (1.9b) have the following form for both $u = P$ or $u = N$:

$$\beta_u^0(x) = m_u^0 e^{-z_u b_u^0 x} + k_u^0 e^{z_u a_u^0 x}, \quad \gamma_u^0(x) = m_u^0 u^m e^{-z_u b_u^0 x}, \tag{2.1a}$$

$$\beta_u^1(x) = m_u^1 e^{-z_u b_u^1 x} + k_u^1 e^{z_u a_u^1 x}, \quad \gamma_u^1(x) = k_u^1 u^m e^{z_u a_u^1 x}, \tag{2.1b}$$

with the following hypotheses on the transfer coefficients:

$$a_u^0, b_u^0, a_u^1, b_u^1 \in [0,1] \text{ for } u = N, P, \tag{2.2}$$

Please cite this article in press as: C. Bataillon et al., Numerical methods for the simulation of a corrosion model with moving oxide layer, J. Comput. Phys. (2012), http://dx.doi.org/10.1016/j.jcp.2012.06.005

and on the interface kinetic constants:

$$m_u^0, k_u^0, m_u^1, k_u^1 > 0. \tag{2.3}$$

Moreover, we assume that

$$3P^m - N^m + \rho_{hl} = 0. \tag{2.4}$$

Remark 2.1. In the applications, we have $\rho_{hl} = -5$, $P^m = 2$ and $N^m = 1$, so that hypothesis (2.4) is satisfied. Then it is expected that the solution to the corrosion model verifies $0 \leqslant P \leqslant P^m$ and $0 \leqslant N \leqslant N^m$. Therefore, it is crucial to design schemes that satisfy these stability properties.

In order to write a finite volume scheme for this system, we first introduce notations concerning the mesh and the time step. We consider a mesh for the domain $[0,1]$, which is not necessarily uniform, i.e., a family of given points $(x_i)_{0\leqslant i\leqslant I+1}$ satisfying

$$x_0 = 0 < x_1 < x_2 < \cdots < x_I < x_{I+1} = 1.$$

Then, for $1 \leqslant i \leqslant I-1$, we define $x_{i+\frac{1}{2}} = \frac{x_i + x_{i+1}}{2}$ and we set $x_{\frac{1}{2}} = x_0 = 0$, $x_{I+\frac{1}{2}} = x_{I+1} = 1$. The cells of the mesh are the intervals $\left(x_{i-\frac{1}{2}}, x_{i+\frac{1}{2}}\right)$ for $1 \leqslant i \leqslant I$. Let us set

$$h_i = x_{i+\frac{1}{2}} - x_{i-\frac{1}{2}}, \quad \text{for } 1 \leqslant i \leqslant I,$$
$$h_{i+\frac{1}{2}} = x_{i+1} - x_i, \quad \text{for } 0 \leqslant i \leqslant I$$

and $h = \max\{h_i, 1 \leqslant i \leqslant I\}$ is the size of the mesh. The time step is denoted by Δt.

The numerical scheme will be Euler implicit in time and finite volume in space. The choice of Euler implicit discretization in time is sensible for convection–diffusion equations in order to avoid a restrictive condition linking time step and mesh size. However, for the discretization of Eqs. (1.1a) and (1.2a), different choices can be made for the time approximation of the electrical field $\partial_x \Psi$. In the sequel, we propose two possibilities leading to two different schemes.

2.1.1. A decoupled scheme

The scheme writes:

$$-\lambda^2\left(d\Psi_{i+\frac{1}{2}}^n - d\Psi_{i-\frac{1}{2}}^n\right) = h_i\left(3P_i^n - N_i^n + \rho_{hl}\right), \quad 1 \leqslant i \leqslant I, \tag{2.5a}$$

$$\varepsilon_u h_i \frac{u_i^{n+1} - u_i^n}{\Delta t} + \mathcal{F}_{u,i+\frac{1}{2}}^{n+1} - \mathcal{F}_{u,i-\frac{1}{2}}^{n+1} = 0, \quad 1 \leqslant i \leqslant I, \text{ for } u = P, N, \tag{2.5b}$$

with the numerical fluxes

$$d\Psi_{i+\frac{1}{2}}^n = \frac{\Psi_{i+1}^n - \Psi_i^n}{h_{i+\frac{1}{2}}}, \quad 0 \leqslant i \leqslant I, \tag{2.6a}$$

$$\mathcal{F}_{u,i+\frac{1}{2}}^{n+1} = \frac{B(z_u h_{i+\frac{1}{2}} d\Psi_{i+\frac{1}{2}}^n) u_i^{n+1} - B\left(-z_u h_{i+\frac{1}{2}} d\Psi_{i+\frac{1}{2}}^n\right) u_{i+1}^{n+1}}{h_{i+\frac{1}{2}}}, \quad 0 \leqslant i \leqslant I, \text{ for } u = P, N, \tag{2.6b}$$

where the function B is the Bernoulli function, leading to Scharfetter–Gummel fluxes:

$$B(x) = \frac{x}{e^x - 1} \text{ for } x \neq 0, \quad B(0) = 1. \tag{2.7}$$

The scheme must be supplemented with the discretization of the boundary conditions and of the initial conditions. For the discretization of the boundary conditions (1.4b), (1.4c), (1.8b), (1.8c), we write:

$$\Psi_0^n - \alpha_0 d\Psi_{\frac{1}{2}}^n = \Delta\Psi_0^{pzc}, \tag{2.8a}$$
$$\Psi_{I+1}^n + \alpha_1 d\Psi_{I+\frac{1}{2}}^n = V - \Delta\Psi_1^{pzc}, \tag{2.8b}$$
$$-\mathcal{F}_{u,\frac{1}{2}}^{n+1} = r_u^0(u_0^{n+1}, \Psi_0^n) = \beta_u^0(\Psi_0^n) u_0^{n+1} - \gamma_u^0(\Psi_0^n), \quad \text{for } u = P, N, \tag{2.8c}$$
$$\mathcal{F}_{u,I+\frac{1}{2}}^{n+1} = r_u^1(u_{I+1}^{n+1}, \Psi_{I+1}^n, V) = \beta_u^1(V - \Psi_{I+1}^n) u_{I+1}^{n+1} - \gamma_u^1(V - \Psi_{I+1}^n), \quad \text{for } u = P, N \tag{2.8d}$$

and for the initial condition

$$u_i^0 = \frac{1}{h_i} \int_{x_{i-\frac{1}{2}}}^{x_{i+\frac{1}{2}}} u^0(x) dx, \quad \text{for } u = P, N. \tag{2.9}$$

The scheme (2.5)–(2.9) will be denoted by $(\mathcal{S}_{dec})$ in all the sequel. It is decoupled in the following sense:

- Starting from $(\mathbf{P}^n, \mathbf{N}^n) = (P_i^n, N_i^n)_{0\leqslant i\leqslant I+1}$, $\mathbf{\Psi}^n = (\Psi_i^n)_{0\leqslant i\leqslant I+1}$ is defined as the solution of the linear system (2.5a), (2.6a), (2.8a), (2.8b).

- Then, knowing $\mathbf{\Psi}^n$, $(\mathbf{P}^{n+1},\mathbf{N}^{n+1})$ is defined as the solution of the linear system (2.5b), (2.6b), (2.7), (2.8c), (2.8d).

In Section 2.2, we will prove the invertibility of the involved linear systems and study the stability of $(\mathcal{S}_{dec})$.

Remark 2.2. If we want to replace the Scharfetter–Gummel fluxes by classical upwind fluxes, we just need to change the B function and choose:

$$B(x) = 1 + x^-, \text{ where } x^- = \max(-x, 0).$$

In fact, the Bernoulli function could be replaced by any function satisfying the three following properties: $B(0) = 1$, $B(x) \geqslant 0$ for all $x \in \mathbb{R}$ and $B(x) - B(-x) = -x$ for all $x \in \mathbb{R}$ (see for instance Ref. [13]). But, with the Bernoulli function, the scheme may be second order in space [14,15].

2.1.2. A fully implicit scheme

The only difference in the fully implicit scheme is in the definition of the numerical fluxes and of the boundary conditions for P and N. Indeed, we replace (2.6b) by

$$\mathcal{F}^{n+1}_{u,i+\frac{1}{2}} = \frac{B\left(z_u h_{i+\frac{1}{2}} d\Psi^{n+1}_{i+\frac{1}{2}}\right) u^{n+1}_i - B\left(-z_u h_{i+\frac{1}{2}} d\Psi^{n+1}_{i+\frac{1}{2}}\right) u^{n+1}_{i+1}}{h_{i+\frac{1}{2}}}, \quad 0 \leqslant i \leqslant I, \quad \text{for } u = P, N \tag{2.10}$$

and (2.8c) and (2.8d) by

$$-\mathcal{F}^{n+1}_{u,\frac{1}{2}} = r^0_u\left(u^{n+1}_0, \Psi^{n+1}_0\right), \quad \text{for } u = P, N, \tag{2.11a}$$

$$\mathcal{F}^{n+1}_{u,I+\frac{1}{2}} = r^1_u(u^{n+1}_{I+1}, \Psi^{n+1}_{I+1}, V), \quad \text{for } u = P, N. \tag{2.11b}$$

The new scheme will be denoted in all the sequel by $(\mathcal{S}_{fi})$.

At each time step, the vector of unknowns $(\mathbf{P}^{n+1}, \mathbf{N}^{n+1}, \mathbf{\Psi}^{n+1}) = \left(P^{n+1}_i, N^{n+1}_i, \Psi^{n+1}_i\right)_{0\leqslant i\leqslant I+1}$ is defined as the solution of a nonlinear system of equations. In Section 2.3, we will prove the existence of a solution to this nonlinear system and investigate the stability of $(\mathcal{S}_{fi})$.

2.2. Stability analysis of a decoupled scheme

Proposition 2.3. *Under the hypotheses (2.1)–(2.3), the scheme $(\mathcal{S}_{dec})$ admits a unique solution $(\mathbf{P}^n,\mathbf{N}^n,\mathbf{\Psi}^n)_{n\geqslant 0}$. Moreover, if $P^0,N^0 \in L^\infty(0,1)$ satisfy $P^0,N^0 \geqslant 0$ almost everywhere on $(0,1)$, then $P^n_i, N^n_i \geqslant 0$ for all $0 \leqslant i \leqslant I+1$ and $n \geqslant 0$.*

Proof. Let us first note that $(\mathbf{P}^0,\mathbf{N}^0)$ is well defined by (2.9) and satisfies the nonnegativity condition. Assume now that for any $n \geqslant 0$, $(\mathbf{P}^n,\mathbf{N}^n)$ is given and satisfies the nonnegativity assumption. Then $\mathbf{\Psi}^n$ is defined as the solution of the linear system (2.5a), (2.6a), (2.8a), (2.8b). The matrix of this linear system is a tridiagonal matrix. As α_0 and α_1 are strictly positive, this matrix is semistrictly diagonally dominant and thus invertible.

Knowing $\mathbf{\Psi}^n$, $\mathbf{P}^{n+1}$ and $\mathbf{N}^{n+1}$ are also defined as solutions of some linear systems. For $u = P,N$ the linear system defined by (2.5b), (2.6b), (2.8c), (2.8d) rewrites:

$$\mathbb{M}^n_u \mathbf{u}^{n+1} = \mathbf{S}^n_u. \tag{2.12}$$

The matrix $\mathbb{M}^n_u \in \mathcal{M}_{I+2}(\mathbb{R})$ is a tridiagonal matrix, whose nonzero terms are defined by:

$$\left(\mathbb{M}^n_u\right)_{ii} = \varepsilon_u \frac{h_i}{\Delta t} + \frac{B\left(z_u h_{i+\frac{1}{2}} d\Psi^n_{i+\frac{1}{2}}\right)}{h_{i+\frac{1}{2}}} + \frac{B\left(-z_u h_{i-\frac{1}{2}} d\Psi^n_{i-\frac{1}{2}}\right)}{h_{i-\frac{1}{2}}}, \quad \forall 1 \leqslant i \leqslant I,$$

$$\left(\mathbb{M}^n_u\right)_{ii+1} = -\frac{B\left(-z_u h_{i+\frac{1}{2}} d\Psi^n_{i+\frac{1}{2}}\right)}{h_{i+\frac{1}{2}}}, \quad \forall 1 \leqslant i \leqslant I,$$

$$\left(\mathbb{M}^n_u\right)_{ii-1} = -\frac{B\left(z_u h_{i-\frac{1}{2}} d\Psi^n_{i-\frac{1}{2}}\right)}{h_{i-\frac{1}{2}}}, \quad \forall 1 \leqslant i \leqslant I,$$

$$\left(\mathbb{M}^n_u\right)_{00} = \frac{B\left(z_u h_{\frac{1}{2}} d\Psi^n_{\frac{1}{2}}\right)}{h_{\frac{1}{2}}} + \beta^0_u(\Psi^n_0),$$

Please cite this article in press as: C. Bataillon et al., Numerical methods for the simulation of a corrosion model with moving oxide layer, J. Comput. Phys. (2012), http://dx.doi.org/10.1016/j.jcp.2012.06.005

$$(\mathbb{M}_u^n)_{01} = -\frac{B\left(-z_u h_{\frac{1}{2}} d\Psi_{\frac{1}{2}}^n\right)}{h_{\frac{1}{2}}},$$
$$(\mathbb{M}_u^n)_{I+1I+1} = \frac{B\left(-z_u h_{I+\frac{1}{2}} d\Psi_{I+\frac{1}{2}}^n\right)}{h_{I+\frac{1}{2}}} + \beta_u^1(V - \Psi_{I+1}^n),$$
$$(\mathbb{M}_u^n)_{I+1I} = -\frac{B\left(z_u h_{I+\frac{1}{2}} d\Psi_{I+\frac{1}{2}}^n\right)}{h_{I+\frac{1}{2}}}.$$

As $\varepsilon_u > 0$ and the functions β_u^0, β_u^1 and B are nonnegative, the matrix $\mathbb{M}_u^n$ has positive diagonal terms and nonpositive off-diagonal terms. Moreover, it is strictly diagonally dominant with respect to its columns. Therefore, $\mathbb{M}_u^n$ is an M-matrix: it is invertible and $(\mathbb{M}_u^n)^{-1} \geqslant 0$. It yields the existence of a unique solution to (2.12).

The right hand side of the linear system (2.12), $\mathbf{S}_u^n$, is defined by:

$$(\mathbf{S}_u^n)_i = \varepsilon_u \tfrac{h_i}{\Delta t} u_i^n, \forall 1 \leqslant i \leqslant I,$$
$$(\mathbf{S}_u^n)_0 = \gamma_u^0(\Psi_0^n), \quad (\mathbf{S}_u^n)_{I+1} = \gamma_u^1(V - \Psi_{I+1}^n).$$

As $u_i^n \geqslant 0$ for $1 \leqslant i \leqslant I$ and γ_u^0, γ_u^1 are nonnegative functions, $\mathbf{S}_u^n$ is a positive-valued vector and as $(\mathbb{M}_u^n)^{-1} \geqslant 0$, we get that $u_i^{n+1} \geqslant 0$ for all $0 \leqslant i \leqslant I+1$. It concludes the proof of Proposition 2.3 by induction. □

Proposition 2.4. *Assume (2.1)–(2.4) and that $P^0, N^0 \in L^\infty(0,1)$ satisfy $0 \leqslant P^0 \leqslant P^m$ and $0 \leqslant N^0 \leqslant N^m$ almost everywhere on $(0,1)$. Then, if $\Delta\Psi_0^{pzc}$ and $\Delta\Psi_1^{pzc}$ fulfill:*

$$-\frac{1}{3a_P^0}\left(1 + \log\left(\alpha_0 a_P^0 k_P^0\right)\right) \leqslant \Delta\Psi_0^{pzc} \leqslant \frac{1}{a_N^0}\left(1 + \log\left(\alpha_0 a_N^0 k_N^0\right)\right), \tag{2.13a}$$
$$-\frac{1}{b_N^1}\left(1 + \log\left(\alpha_1 b_N^1 m_N^1\right)\right) \leqslant \Delta\Psi_1^{pzc} \leqslant \frac{1}{3b_P^1}\left(1 + \log\left(\alpha_1 b_P^1 m_P^1\right)\right), \tag{2.13b}$$

and if the following inequality on the time step holds:

$$\Delta t \leqslant \min\left(\frac{\lambda^2}{9P^m}, \frac{D_1}{D_2}\frac{\lambda^2}{N^m}\right), \tag{2.14}$$

then the solution to the scheme $(\mathcal{S}_{dec})$ satisfies

$$0 \leqslant P_i^n \leqslant P^m \text{ and } 0 \leqslant N_i^n \leqslant N^m \quad \forall 0 \leqslant i \leqslant I+1, \forall n \geqslant 0. \tag{2.15}$$

Proof. First, we note that the hypotheses on the initial conditions ensure that (2.15) is satisfied for $n = 0$. We now assume that (2.15) is verified for $n \geqslant 0$ and prove that it also holds for $n+1$. The nonnegativity has already been proven.

Let us first compute the product $\mathbb{M}_u^n \mathbf{u}^m$, where $\mathbf{u}^m$ is the constant vector of $\mathbb{R}^{I+2}$, whose components are all equal to the same value u^m. As the Bernoulli function defined by (2.7) satisfies $B(x) - B(-x) = -x$ for all $x \in \mathbb{R}$, we have

$$(\mathbb{M}_u^n \mathbf{u}^m)_i = u^m\left(\varepsilon_u \frac{h_i}{\Delta t} - z_u\left(d\Psi_{i+\frac{1}{2}}^n - d\Psi_{i-\frac{1}{2}}^n\right)\right), \quad \forall 1 \leqslant i \leqslant I,$$
$$(\mathbb{M}_u^n \mathbf{u}^m)_0 = u^m\left(-z_u d\Psi_{\frac{1}{2}}^n + \beta_u^0(\Psi_0^n)\right),$$
$$(\mathbb{M}_u^n \mathbf{u}^m)_{I+1} = u^m\left(z_u d\Psi_{I+\frac{1}{2}}^n + \beta_u^1(V - \Psi_{I+1}^n)\right).$$

Using (2.5a), (2.8a), (2.8b), it rewrites

$$(\mathbb{M}_u^n \mathbf{u}^m)_i = u^m\left(\varepsilon_u \frac{h_i}{\Delta t} + \frac{z_u h_i}{\lambda^2}(3P_i^n - N_i^n + \rho_{hl})\right), \quad \forall 1 \leqslant i \leqslant I,$$
$$(\mathbb{M}_u^n \mathbf{u}^m)_0 = u^m\left(-\frac{z_u}{\alpha_0}(\Psi_0^n - \Delta\Psi_0^{pzc}) + \beta_u^0(\Psi_0^n)\right),$$
$$(\mathbb{M}_u^n \mathbf{u}^m)_{I+1} = u^m\left(\frac{z_u}{\alpha_1}(V - \Delta\Psi_1^{pzc} - \Psi_{I+1}^n) + \beta_u^1(V - \Psi_{I+1}^n)\right).$$

Using (2.4), it yields

$$\left(\mathbb{M}_u^n(\mathbf{u}^{n+1}-\mathbf{u}^m)\right)_i = \varepsilon_u\frac{h_i}{\Delta t}(u_i^n-u^m) - \frac{z_u h_i}{\lambda^2}u^m\left(3(P_i^n-P^m)-(N_i^n-N^m)\right) \quad \forall 1\leqslant i\leqslant I,$$
$$\left(\mathbb{M}_u^n(\mathbf{u}^{n+1}-\mathbf{u}^m)\right)_0 = \gamma_u^0(\Psi_0^n) - u^m\left(-\frac{z_u}{\alpha_0}(\Psi_0^n-\Delta\Psi_0^{pzc})+\beta_u^0(\Psi_0^n)\right),$$
$$\left(\mathbb{M}_u^n(\mathbf{u}^{n+1}-\mathbf{u}^m)\right)_{I+1} = \gamma_u^1(V-\Psi_{I+1}^n) - u^m\left(\frac{z_u}{\alpha_1}(V-\Delta\Psi_1^{pzc}-\Psi_{I+1}^n)+\beta_u^1(V-\Psi_{I+1}^n)\right).$$

We now apply these results to $u = P$ and N, with respectively $u^m = P^m$, $\mathbf{u}^m = \mathbf{P}^m$, and $u^m = N^m$, $\mathbf{u}^m = \mathbf{N}^m$. For the inner terms, we get $\forall 1\leqslant i\leqslant I$:

$$\left(\mathbb{M}_P^n(\mathbf{P}^{n+1}-\mathbf{P}^m)\right)_i = \frac{h_i}{\Delta t}(P_i^n-P^m)\left(1-\frac{9\Delta t}{\lambda^2}P^m\right)+\frac{3P^m h_i}{\lambda^2}(N_i^n-N^m),$$
$$\left(\mathbb{M}_N^n(\mathbf{N}^{n+1}-\mathbf{N}^m)\right)_i = \frac{h_i}{\Delta t}(N_i^n-N^m)\left(\frac{D_1}{D_2}-\frac{\Delta t}{\lambda^2}N^m\right)+\frac{3N^m h_i}{\lambda^2}(P_i^n-P^m).$$

Therefore, if Δt verifies (2.14), we have $(\mathbb{M}_P^n(\mathbf{P}^{n+1}-\mathbf{P}^m))_i \leqslant 0$ and $\left(\mathbb{M}_N^n(\mathbf{N}^{n+1}-\mathbf{N}^m)\right)_i \leqslant 0$ for all $1\leqslant i\leqslant I$. It remains to prove that $\left(\mathbb{M}_u^n(\mathbf{u}^{n+1}-\mathbf{u}^m)\right)_0 \leqslant 0$, $\left(\mathbb{M}_u^n(\mathbf{u}^{n+1}-\mathbf{u}^m)\right)_{I+1} \leqslant 0$ for $u = P,N$. But, $\left(\mathbb{M}_u^n(\mathbf{u}^{n+1}-\mathbf{u}^m)\right)_0 = \xi_u^0(\Psi_0^n)$ and $\left(\mathbb{M}_u^n(\mathbf{u}^{n+1}-\mathbf{u}^m)\right)_{I+1} = \xi_u^1(V-\Psi_{I+1}^n)$, with

$$\xi_u^0(x) = \gamma_u^0(x) - u^m\beta_u^0(x) + u^m\frac{z_u}{\alpha_0}x - u^m\frac{z_u}{\alpha_0}\Delta\Psi_0^{pzc},$$
$$\xi_u^1(x) = \gamma_u^1(x) - u^m\beta_u^1(x) - u^m\frac{z_u}{\alpha_1}x + u^m\frac{z_u}{\alpha_1}\Delta\Psi_1^{pzc}.$$

Using the definitions (2.1), we get

$$\xi_u^0(x) = -u^m k_u^0 e^{z_u a_u^0 x} + u^m\frac{z_u}{\alpha_0}x - u^m\frac{z_u}{\alpha_0}\Delta\Psi_0^{pzc},$$
$$\xi_u^1(x) = -u^m m_u^1 e^{-z_u b_u^1 x} - u^m\frac{z_u}{\alpha_1}x + u^m\frac{z_u}{\alpha_1}\Delta\Psi_1^{pzc}.$$

The study of the variations of ξ_u^0 and ξ_u^1 for $u = N,P$ shows that these functions are always increasing on an interval $(-\infty,\bar{x}]$ and then decreasing on $[\bar{x},+\infty)$. Therefore they reach a maximum value and the hypotheses (2.13b) ensure that the maximum value is always nonpositive. Then ξ_P^0, ξ_P^1, ξ_N^0, ξ_N^1 are nonpositive functions on $\mathbb{R}$.

Finally, we get that $\left(\mathbb{M}_P^n(\mathbf{P}^{n+1}-\mathbf{P}^m)\right)_i \leqslant 0$ and $\left(\mathbb{M}_N^n(\mathbf{N}^{n+1}-\mathbf{N}^m)\right)_i \leqslant 0$ for all $0\leqslant i\leqslant I+1$. As $\mathbb{M}_P^n$ and $\mathbb{M}_N^n$ are M-matrices, it concludes the proof of Proposition 2.4. □

In the applications, we have $\lambda^2\approx 10^{-6}$ and $\frac{D_1}{D_2}\approx 10^{-14}$, so that the hypothesis on Δt, (2.14), imposes $\Delta t\approx 10^{-20}$. It makes the decoupled scheme unusable in practice and motivates the study of the fully implicit scheme.

2.3. Stability analysis of a fully implicit scheme

The scheme $(\mathcal{S}_{fi})$ is defined as a set of nonlinear equations at each time step. We need to prove the existence of a solution to the nonlinear system of equations and to study the stability of the scheme.

Proposition 2.5. *Assume (2.1)–(2.4) and that $P^0,N^0\in L^\infty(0,1)$ satisfy $0\leqslant P^0\leqslant P^m$ and $0\leqslant N^0\leqslant N^m$ almost everywhere on (0,1). Then, there exists a solution to the fully implicit scheme $(\mathcal{S}_{fi})$: $((\mathbf{P}^n,\mathbf{N}^n)_{n\geqslant 0},(\mathbf{\Psi}^n)_{n\geqslant 1})$. Furthermore, if $\Delta\Psi_0^{pzc}$ and $\Delta\Psi_1^{pzc}$ verify (2.13b), the solution to the scheme $(\mathcal{S}_{fi})$ satisfies the stability property (2.15).*

Proof. In order to prove Proposition 2.5, we adapt some ideas developed by Prohl and Schmuck in [16].

First, we note that $(\mathbf{P}^0,\mathbf{N}^0)$ is well defined by (2.9) and satisfies (2.15). Assume now that for any $n\geqslant 0$, $(\mathbf{P}^n,\mathbf{N}^n,\mathbf{\Psi}^n)$ is given and satisfies (2.15). Then, we will prove that there exists a solution $(\mathbf{P}^{n+1},\mathbf{N}^{n+1},\mathbf{\Psi}^{n+1})$ to $(\mathcal{S}_{fi})$ and that

$$0\leqslant P_i^{n+1}\leqslant P^m \text{ and } 0\leqslant N_i^{n+1}\leqslant N^m \quad \forall 0\leqslant i\leqslant I+1.$$

Therefore, let us consider the mapping

$$\mathcal{T}_n^\mu:\quad \mathbb{R}^{I+2}\times\mathbb{R}^{I+2} \;\to\; \mathbb{R}^{I+2}\times\mathbb{R}^{I+2}$$
$$(\mathbf{P},\mathbf{N})\mapsto(\widetilde{\mathbf{P}},\widetilde{\mathbf{N}})$$

defined, for $\mu > 0$, by

$$-\lambda^2\left(d\Psi_{i+\frac{1}{2}}-d\Psi_{i-\frac{1}{2}}\right) = h_i(3P_i-N_i+\rho_{hl}),\quad 1\leqslant i\leqslant I,$$
$$\Psi_0-\alpha_0 d\Psi_{\frac{1}{2}} = \Delta\Psi_0^{pzc},$$
$$\Psi_{I+1}+\alpha_1 d\Psi_{I+\frac{1}{2}} = V-\Delta\Psi_1^{pzc},$$

$$\varepsilon_u \frac{h_i}{\Delta t}\left(\left(1+\frac{\mu}{\varepsilon_u\lambda^2}\right)\tilde{u}_i - \frac{\mu}{\varepsilon_u\lambda^2}u_i - u_i^n\right) + \mathcal{F}_{u,i+\frac{1}{2}} - \mathcal{F}_{u,i-\frac{1}{2}} = 0, \quad 1 \leqslant i \leqslant I, \text{ for } u = P, N,$$

$$\mathcal{F}_{u,i+\frac{1}{2}} = \frac{B\left(z_u h_{i+\frac{1}{2}} d\Psi_{i+\frac{1}{2}}\right)\tilde{u}_i - B\left(-z_u h_{i+\frac{1}{2}} d\Psi_{i+\frac{1}{2}}\right)\tilde{u}_{i+1}}{h_{i+\frac{1}{2}}}, \quad 0 \leqslant i \leqslant I, \text{ for } u = P, N,$$

$$-\mathcal{F}_{u,\frac{1}{2}} = r_u^0(\tilde{u}_0, \Psi_0) = \beta_u^0(\Psi_0)\tilde{u}_0^{n+1} - \gamma_u^0(\Psi_0), \quad \text{for } u = P, N,$$

$$\mathcal{F}_{u,I+\frac{1}{2}} = r_u^1(\tilde{u}_{I+1}, \Psi_{I+1}, V) = \beta_u^1(V - \Psi_{I+1})\tilde{u}_{I+1} - \gamma_u^1(V - \Psi_{I+1}), \quad \text{for } u = P, N.$$

This mapping $\mathcal{T}_n^\mu$ is defined by two successive steps:

- the first step defines an intermediate vector $\boldsymbol{\Psi}$ as the solution of a linear system of equations,
- the second step defines $\widetilde{\mathbf{P}}$ and $\widetilde{\mathbf{N}}$ as solutions of linear systems of equations, very close to the systems involved in the decoupled scheme (there is an additional term on the diagonal of the matrices and the right-hand-sides are slightly modified).

Therefore, it is a continuous mapping from $\mathbb{R}^{I+2} \times \mathbb{R}^{I+2}$ to itself. Applying the proof of stability of Proposition 2.4, we obtain that $\mathcal{T}_n^\mu$ preserves the set:

$$\mathcal{K} = \{(\mathbf{P}, \mathbf{N}) \in \mathbb{R}^{\mathbf{I+2}} \times \mathbb{R}^{\mathbf{I+2}}; \quad \mathbf{0} \leqslant \mathbf{P_i} \leqslant \mathbf{P^m}, \ \mathbf{0} \leqslant \mathbf{N_i} \leqslant \mathbf{N^m}, \ \forall\, \mathbf{0} \leqslant \mathbf{i} \leqslant \mathbf{I+1}\}$$

as long as (2.13b) is satisfied and Δt verifies:

$$\Delta t \leqslant \mu \min\left(\frac{1}{9P^m}, \frac{1}{N^m}\right).$$

Then, thanks to Brouwer's theorem, we conclude that $\mathcal{T}_n^\mu$ has a fixed point in $\mathcal{K}$. Moreover, this fixed point, with the corresponding $\boldsymbol{\Psi}$, is a solution to the scheme $(\mathcal{S}_{fi})$. It shows the existence of a solution to the scheme and the stability properties (2.15). As this result holds for any μ, the scheme is unconditionally stable. □

Remark 2.6. With the Brouwer fixed point theorem, we get the existence of one solution to the scheme $(\mathcal{S}_{fi})$ but we do not get any information on uniqueness. This question of uniqueness is relevant but still open. Therefore, in the sequel, the solution to the numerical scheme will be the one selected by Newton's method used to solve the nonlinear system of equations $(\mathcal{S}_{fi})$. During the numerical experiments we did not encounter situations hinting at multiple solutions.

3. Numerical schemes for the complete corrosion model

3.1. Change of variables

The corrosion model involves moving boundaries through (1.5). The system of equations is defined on the space–time domain $\bigcup_{0\leqslant t\leqslant T}[X_0(t), X_1(t)] \times \{t\}$. The size of the domain at time t is $L(t) = X_1(t) - X_0(t)$. An Eulerian description is chosen in order to handle the motion of the boundaries; the physical spatial domain is substituted by a computational one. Therefore, we introduce the following change of variables:

$$(x,t) \mapsto \left(\xi(x,t) = \frac{x - X_0(t)}{X_1(t) - X_0(t)}, t\right)$$

$$\bigcup_{0\leqslant t\leqslant T}[X_0(t), X_1(t)] \times \{t\} \to [0,1] \times [0,T]$$

and to every function u (respectively Ψ) defined on $\bigcup_{0\leqslant t\leqslant T}[X_0(t), X_1(t)] \times \{t\}$ we associate a function $\bar{u}$ (respectively $\overline{\Psi}$) defined on $[0,1] \times [0,T]$ such that $u(x,t) = \bar{u}(\xi(x,t), t)$ (respectively $\Psi(x,t) = \overline{\Psi}(\xi(x,t), t)$). Then, we have:

$$\partial_t u = \partial_t \bar{u} - \frac{1}{L(t)}\left(X_0'(t) + \xi L'(t)\right)\partial_\xi \bar{u}$$

$$J_u = \frac{1}{L(t)}\left(-\partial_\xi \bar{u} - z_u \bar{u}\partial_\xi \overline{\Psi}\right) = \frac{1}{L(t)} J_{\bar{u}}.$$

But, using the fact that $\xi\partial_\xi \bar{u} = \partial_\xi(\xi\bar{u}) - \bar{u}$, we get

$$\partial_t u = \frac{1}{L(t)}\left(\partial_t(L(t)\bar{u}) - \partial_\xi\left(\left(X_0'(t) + \xi L'(t)\right)\bar{u}\right)\right).$$

Finally, forgetting the bars, the convection–diffusion equation with boundary conditions (1.8) rewrites in the new variables:

$$\varepsilon_u L(t)\partial_t(L(t)u) + \partial_\xi J_u - \varepsilon_u \partial_\xi\big(L(t)\big(X_0'(t) + \xi L'(t)\big)u\big) = 0,$$

$$J_u = -\partial_\xi u - z_u u \partial_\xi \Psi, \quad \xi \in (0,1) \tag{3.1a}$$

$$-J_u - \varepsilon_u u L(t) X_0'(t) = L(t) r_u^0(u,\Psi), \quad \xi = 0 \tag{3.1b}$$

$$J_u + \varepsilon_u u L(t) X_1'(t) = L(t) r_u^1(u,\Psi,V), \quad \xi = 1. \tag{3.1c}$$

We note that in the new variables, the convection–diffusion equation (3.1a) contains an additional convection term coming from the displacement of the interfaces. Therefore, (3.1c) is equivalent to the following formulation:

$$\varepsilon_u L(t)\partial_t(L(t)u) + \partial_\xi \widehat{J}_u = 0,$$

$$\widehat{J}_u = -\partial_\xi u - \big(z_u \partial_\xi \Psi + \varepsilon_u L(t)(X_0'(t) + \xi L'(t))\big)u, \quad \xi \in (0,1), \tag{3.2a}$$

$$-\widehat{J}_u = L(t) r_u^0(u,\Psi), \quad \xi = 0, \tag{3.2b}$$

$$\widehat{J}_u = L(t) r_u^1(u,\Psi,V), \quad \xi = 1. \tag{3.2c}$$

The equation on the electrostatic potential (1.4) rewrites in the new variables:

$$-\frac{\lambda^2}{L(t)^2}\partial_{\xi\xi}^2 \Psi = P - N + 2C + \rho_{hl}, \quad \xi \in (0,1), \tag{3.3a}$$

$$\Psi - \frac{\alpha_0}{L(t)}\partial_\xi \Psi = \Delta\Psi_0^{pzc}, \quad \xi = 0, \tag{3.3b}$$

$$\Psi + \frac{\alpha_1}{L(t)}\partial_\xi \Psi = V - \Delta\Psi_1^{pzc}, \quad x = 1. \tag{3.3c}$$

Finally, the full DPCM model (1.1)–(1.5) rewritten on the fixed domain is given by (3.2) applied for $u = N,P,C$, (3.3) and the moving boundary equations:

$$\frac{dX_0}{dt} = v_d^0(t) + \frac{dX_1}{dt}\left(1 - \frac{\Omega_{ox}}{m\Omega_{Fe}}\right), \tag{3.4a}$$

$$\frac{dX_1}{dt} = -\frac{D_3}{4D_1}\frac{\Omega_{Fe}}{\Omega_{ox}}\frac{\widehat{J}_C(1)}{L(t)} = -\frac{D_3}{4D_1}\frac{\Omega_{Fe}}{\Omega_{ox}} r_C^1(C(1,t),\Psi(1,t),V), \tag{3.4b}$$

$$\text{with } v_d^0(t) = k_d^0 e^{-5a_d^0\Psi(0,t)}, \quad \forall t \geqslant 0. \tag{3.4c}$$

3.2. Numerical scheme

The comparison of the decoupled and the implicit schemes on the simplified two-species model has shown the superiority of the fully implicit scheme $(\mathcal{S}_{fi})$ with respect to stability. Another motivation for this choice comes from the fact that it has been proven that for this type of schemes, monotone and exponential decay of the free energy to its equilibrium value can be shown for both the continuous and discretized versions of the problem [17]. In this sense, the scheme has the potential to reproduce important physical properties on the discrete level. Let us now adapt the scheme $(\mathcal{S}_{fi})$ to the new system of equations (3.2) (for $u = N,P,C$), (3.3). with the moving boundary equations (3.4). The notations for the mesh are the same as in Section 2 but with the points denoted by $(\xi_i)_{0\leqslant i\leqslant I+1}$ instead of $(x_i)_{0\leqslant i\leqslant I+1}$. Let Δt be the time step.

The unknowns of the scheme are:

- the densities $(N_i^n, P_i^n, C_i^n)_{0\leqslant i\leqslant I+1, n\geqslant 0}$ and the electrostatic potential $(\Psi_i^n)_{0\leqslant i\leqslant I+1, n\geqslant 1}$,
- the position of the interfaces $(X_0^n, X_1^n)_{n\geqslant 0}$.

The size of the domain $(L^n)_{n\geqslant 0}$ is defined by $L^n = X_1^n - X_0^n$ for all $n \geqslant 0$.

The discretization of Eqs. (3.2a) and (3.3a) leads to:

$$\varepsilon_u L^{n+1} h_i \frac{L^{n+1}u_i^{n+1} - L^n u_i^n}{\Delta t} + \mathcal{G}_{u,i+\frac{1}{2}}^{n+1} - \mathcal{G}_{u,i-\frac{1}{2}}^{n+1} = 0, \quad 1 \leqslant i \leqslant I, \text{ for } u = P,N,C, \tag{3.5a}$$

$$-\frac{\lambda^2}{(L^{n+1})^2}\left(d\Psi_{i+\frac{1}{2}}^{n+1} - d\Psi_{i-\frac{1}{2}}^{n+1}\right) = h_i\left(3P_i^{n+1} - N_i^{n+1} + 2C_i^{n+1} - \rho_{hl}\right), \quad 1 \leqslant i \leqslant I, \tag{3.5b}$$

where the numerical fluxes for Ψ are still given by (2.6a) and for $u = P,N,C$ by

$$\mathcal{G}_{u,i+\frac{1}{2}}^{n+1} = \frac{1}{h_{i+\frac{1}{2}}}\left(B\left(h_{i+\frac{1}{2}}\left(z_u d\Psi_{i+\frac{1}{2}}^{n+1} + \varepsilon_u \mathbf{v}_{i+\frac{1}{2}}^{n+1}\right)\right)u_i^{n+1} - B\left(-h_{i+\frac{1}{2}}\left(z_u d\Psi_{i+\frac{1}{2}}^{n+1} + \varepsilon_u \mathbf{v}_{i+\frac{1}{2}}^{n+1}\right)\right)u_{i+1}^{n+1}\right), \quad 0 \leqslant i \leqslant I, \tag{3.6}$$

Please cite this article in press as: C. Bataillon et al., Numerical methods for the simulation of a corrosion model with moving oxide layer, J. Comput. Phys. (2012), http://dx.doi.org/10.1016/j.jcp.2012.06.005

with the following approximation of the artificial drift velocity:

$$\mathbf{v}_{i+\frac{1}{2}}^{n+1} = L^{n+1}\left(\frac{X_0^{n+1}-X_0^n}{\Delta t} + \xi_{i+\frac{1}{2}}\frac{L^{n+1}-L^n}{\Delta t}\right). \tag{3.7}$$

For the boundary conditions (3.3b), (3.3c), (3.2b), (3.2c), we respectively write:

$$\Psi_0^{n+1} - \frac{\alpha_0}{L^{n+1}} d\Psi_{\frac{1}{2}}^{n+1} = \Delta\Psi_0^{pzc}, \tag{3.8a}$$

$$\Psi_{I+1}^{n+1} + \frac{\alpha_1}{L^{n+1}} d\Psi_{I+\frac{1}{2}}^{n+1} = V - \Delta\Psi_1^{pzc}, \tag{3.8b}$$

$$-\mathcal{G}_{u,\frac{1}{2}}^{n+1} = L^{n+1} r_u^0\left(u_0^{n+1}, \Psi_0^{n+1}\right), \tag{3.8c}$$

$$\mathcal{G}_{u,I+\frac{1}{2}}^{n+1} = L^{n+1} r_u^1\left(u_{I+1}^{n+1}, \Psi_{I+1}^{n+1}\right). \tag{3.8d}$$

For the discretization of the moving interface equations (3.4), two different choices will be studied: either we use an Euler explicit in time scheme for (3.4) or we use an Euler implicit in time scheme.

3.2.1. Explicit scheme for the moving interface equations

In this case, the scheme for (3.4) writes:

$$\frac{X_0^{n+1}-X_0^n}{\Delta t} = k_d^0 e^{-5a_d^0\Psi_0^n} + \frac{X_1^{n+1}-X_1^n}{\Delta t}\left(1-\frac{\Omega_{ox}}{m\Omega_{Fe}}\right), \tag{3.9a}$$

$$\frac{X_1^{n+1}-X_1^n}{\Delta t} = -\frac{D_3}{4D_1}\frac{\Omega_{Fe}}{\Omega_{ox}} r_C^1(C_{I+1}^n, \Psi_{I+1}^n, V), \tag{3.9b}$$

and we define $L^{n+1} = X_1^{n+1} - X_0^{n+1}$.

With this choice of discretization, the computation of $\left(X_0^{n+1}, X_1^{n+1}, L^{n+1}\right)$ is decoupled from the computation of $\left(P_i^{n+1}, N_i^{n+1}, C_i^{n+1}, \Psi_i^{n+1}\right)_{0\leqslant i\leqslant I+1}$ at each time step. In the sequel, the scheme (3.5)–(3.9) will be denoted by $(\mathcal{S}_{tot}^e)$.

3.2.2. Implicit scheme for the moving interface equations

In this case, the scheme for (3.4) writes:

$$\frac{X_0^{n+1}-X_0^n}{\Delta t} = k_d^0 e^{-5a_d^0\Psi_0^{n+1}} + \frac{X_1^{n+1}-X_1^n}{\Delta t}\left(1-\frac{\Omega_{ox}}{m\Omega_{Fe}}\right), \tag{3.10a}$$

$$\frac{X_1^{n+1}-X_1^n}{\Delta t} = -\frac{D_3}{4D_1}\frac{\Omega_{Fe}}{\Omega_{ox}} r_C^1\left(C_{I+1}^{n+1}, \Psi_{I+1}^{n+1}, V\right) \tag{3.10b}$$

and we define $L^{n+1} = X_1^{n+1} - X_0^{n+1}$.

With this choice of discretization for (3.4), the computation of $\left(X_0^{n+1}, X_1^{n+1}, L^{n+1}\right)$ at each time step is completely coupled with the computation of $\left(P_i^{n+1}, N_i^{n+1}, C_i^{n+1}, \Psi_i^{n+1}\right)_{0\leqslant i\leqslant I+1}$. Indeed, the scheme (3.5)–(3.8) and (3.10), which will be denoted in the sequel $\left(\mathcal{S}_{tot}^i\right)$, defines a nonlinear system of equations at each time step, whose unknowns are

$$\left(\left(P_i^{n+1}, N_i^{n+1}, C_i^{n+1}, \Psi_i^{n+1}\right)_{0\leqslant i\leqslant I+1}, X_0^{n+1}, X_1^{n+1}, L^{n+1}\right).$$

3.3. Study of the galvanostatic case

Up to now, we have considered V as a given applied potential (the potentiostatic case). For the galvanostatic case, V is defined by the supplementary Eq. (1.7). From the numerical point of view, this supplementary equation will be approximated by:

$$-3\left(\mathcal{G}_{P,I+\frac{1}{2}}^{n+1} + \frac{D_3}{4D_1}\mathcal{G}_{C,I+\frac{1}{2}}^{n+1}\right) + \frac{D_2}{D_1}\mathcal{G}_{N,I+\frac{1}{2}}^{n+1} = 0 \quad \forall n \geqslant 0. \tag{3.11}$$

It adds one unknown and one nonlinear equation to the previous system of nonlinear equations $\left(\mathcal{S}_{tot}^i\right)$. In the sequel, we will denote this new scheme $\left(\mathcal{S}_{tot}^{i,gc}\right)$.

4. Implementation of the designed numerical methods

4.1. Explicit handling of the boundary positions

We start with the description of the implementation of the scheme $(\mathcal{S}_{tot}^e)$ which involves the explicit handling of the boundary positions. The nonlinear system corresponding to $(\mathcal{S}_{tot}^e)$ is written as:

Please cite this article in press as: C. Bataillon et al., Numerical methods for the simulation of a corrosion model with moving oxide layer, J. Comput. Phys. (2012), http://dx.doi.org/10.1016/j.jcp.2012.06.005

$$G(Y) = 0,$$

where $Y \in \mathbb{R}^{4(I+2)}$ is the vector of unknowns, ordered as follows:

$$Y = \left(\Psi_0^{n+1}, P_0^{n+1}, N_0^{n+1}, C_0^{n+1}, \Psi_1^{n+1}, P_1^{n+1}, N_1^{n+1}, C_1^{n+1}, \dots, \dots\right)^t, \tag{4.1}$$

and G is the function from $\mathbb{R}^{4(I+2)}$ to $\mathbb{R}^{4(I+2)}$ defined by

$$G(Y) = \begin{pmatrix}
\Psi_0^{n+1} - \frac{\alpha_0}{L^{n+1}} d\Psi_{\frac{1}{2}}^{n+1} - \Delta\Psi_0^{pzc} \\
\Delta t \mathcal{G}_{P,\frac{1}{2}}^{n+1} + \Delta t L^{n+1} r_P^0\left(P_0^{n+1}, \Psi_0^{n+1}\right) \\
\Delta t \mathcal{G}_{N,\frac{1}{2}}^{n+1} + \Delta t L^{n+1} r_N^0\left(N_0^{n+1}, \Psi_0^{n+1}\right) \\
\Delta t \mathcal{G}_{C,\frac{1}{2}}^{n+1} + \Delta t L^{n+1} r_C^0\left(C_0^{n+1}, \Psi_0^{n+1}\right) \\
-\frac{\lambda^2}{(L^{n+1})^2}\left(d\Psi_{\frac{3}{2}}^{n+1} - d\Psi_{\frac{1}{2}}^{n+1}\right) - h_1\left(3P_1^{n+1} - N_1^{n+1} + 2C_1^{n+1} - \rho_{hl}\right) \\
\varepsilon_P L^{n+1} h_1\left(L^{n+1}P_1^{n+1} - L^n P_1^n\right) + \Delta t\left(\mathcal{G}_{P,\frac{3}{2}}^{n+1} - \mathcal{G}_{P,\frac{1}{2}}^{n+1}\right) \\
\varepsilon_N L^{n+1} h_1\left(L^{n+1}N_1^{n+1} - L^n N_1^n\right) + \Delta t\left(\mathcal{G}_{N,\frac{3}{2}}^{n+1} - \mathcal{G}_{N,\frac{1}{2}}^{n+1}\right) \\
\varepsilon_C L^{n+1} h_1\left(L^{n+1}C_1^{n+1} - L^n C_1^n\right) + \Delta t\left(\mathcal{G}_{C,\frac{3}{2}}^{n+1} - \mathcal{G}_{C,\frac{1}{2}}^{n+1}\right) \\
\vdots \\
\Psi_{I+1}^{n+1} + \frac{\alpha_1}{L^{n+1}} d\Psi_{I+\frac{1}{2}}^{n+1} - (V - \Delta\Psi_1^{pzc}) \\
\Delta t \mathcal{G}_{P,I+\frac{1}{2}}^{n+1} - \left(\Delta t L^{n+1} r_P^1(P_{I+1}^{n+1}, \Psi_{I+1}^{n+1})\right) \\
\Delta t \mathcal{G}_{N,I+\frac{1}{2}}^{n+1} - \left(\Delta t L^{n+1} r_N^1(N_{I+1}^{n+1}, \Psi_{I+1}^{n+1})\right) \\
\Delta t \mathcal{G}_{C,I+\frac{1}{2}}^{n+1} - \left(\Delta t L^{n+1} r_C^1(C_{I+1}^{n+1}, \Psi_{I+1}^{n+1})\right)
\end{pmatrix}. \tag{4.2}$$

Newton's method is used in order to solve the nonlinear system. This strategy in particular can take advantage of the fact that the solution for t^n can be taken as initial value. The Jacobian matrix, denoted by A, has a band structure, which in a standard manner allows LU factorization. Therefore each linear system in Newton's iteration can be solved in $O(I)$ floating point operations.

4.2. Implicit handling of the boundary positions

We describe the algorithm used to solve the nonlinear system $\left(\mathcal{S}_{tot}^i\right)$ in Section 3.2. A similar algorithm has been implemented for the scheme $\left(\mathcal{S}_{tot}^{i,gc}\right)$ of Section 3.3. The nonlinear system $\left(\mathcal{S}_{tot}^i\right)$ is written as:

$$F(Z) = 0,$$

where $Z \in \mathbb{R}^{4(I+2)+2}$ is the vector of unknowns, ordered as follows:

$$\begin{pmatrix} Y \\ \left(X_0^{n+1}, X_1^{n+1}\right)^t \end{pmatrix}, \tag{4.3}$$

and $F(Z)$ is the function from $\mathbb{R}^{4(I+2)+2}$ to $\mathbb{R}^{4(I+2)+2}$ defined by:

$$F(Z) = \begin{pmatrix} G(Y) \\ \left(X_0^{n+1} - X_0^n\right) - \left(\Delta t k_d^0 e^{-5a_d^0\Psi_0^{n+1}} + \left(X_1^{n+1} - X_1^n\right)\left(1 - \frac{\Omega_{ox}}{m\Omega_{Fe}}\right)\right) \\ \left(X_1^{n+1} - X_1^n\right) + \Delta t \frac{D_3}{4D_1}\frac{\Omega_{Fe}}{\Omega_{ox}} r_C^1\left(C_{I+1}^{n+1}, \Psi_{I+1}^{n+1}, V\right) \end{pmatrix}. \tag{4.4}$$

Again, Newton's method is applied to solve this nonlinear system of equations. The Schur complement technique is applied with the following block decomposition of the Jacobian matrix:

$$J_F(Z) = \left(\begin{array}{c|c} \mathrm{A} & \mathrm{E} \\ \hline \mathrm{F} & \mathrm{D} \end{array}\right) \in \mathcal{M}_{4(I+2)+2} \tag{4.5}$$

with $\mathrm{A} = J_G(Y) \in \mathcal{M}_{4(I+2)}$, $\mathrm{E} \in \mathcal{M}_{4(I+2),2}$, $\mathrm{F} \in \mathcal{M}_{2,4(I+2)}$ and $\mathrm{D} \in \mathcal{M}_2$.

Splitting the unknown vector and the right-hand-side as follows:

Please cite this article in press as: C. Bataillon et al., Numerical methods for the simulation of a corrosion model with moving oxide layer, J. Comput. Phys. (2012), http://dx.doi.org/10.1016/j.jcp.2012.06.005

$$J_F(Z)\begin{pmatrix} w_1 \\ \hline w_2 \end{pmatrix} = \begin{pmatrix} v_1 \\ \hline v_2 \end{pmatrix} \tag{4.6}$$

with w_1 and v_1 in $\in \mathbb{R}^{4(I+2)}$ and w_2 and v_2 in $\in \mathbb{R}^2$, we have:

$$(\mathrm{D} - \mathrm{F}\mathrm{A}^{-1}\mathrm{E})w_2 = v_2 - \mathrm{F}\mathrm{A}^{-1}v_1, \tag{4.7}$$

$$w_1 = \mathrm{A}^{-1}v_1 - \mathrm{A}^{-1}\mathrm{E}w_2. \tag{4.8}$$

Solving (4.7) and (4.8) requires three solutions of linear systems associated to the banded matrix A, whose half-bandwidth is bounded by 7 thanks to the ordering of the unknowns described by (4.1). Thus, the *LU* factorization of the matrix A can be computed in $O(I)$ floating operations, and since all the other computations required for one Newton iteration are (at most) of the same order, the CPU-time for each of these iterations is in $O(I)$.

4.3. Handling of the galvanostatic case

Initially, Eq. (3.11) of the galvanostatic scheme $\left(\mathcal{S}_{tot}^{i,gc}\right)$ has been handled by a fixed point iteration to detect V. After augmenting system (4.4) by Eq. (3.11) and the unknown V, the resulting linear system still can be well handled by the Schur complement approach described in Section 4.2.

4.4. A priori spatial refinement of boundary layers

As the occurrence of boundary layers is a well known feature to be expected for solutions of coupled Nernst–Planck–Poisson equations, an a priori refinement of the spatial mesh in the vicinity of the domain boundaries is performed. The position of the discretization nodes in the domain $[0,1]$ is calculated from the zeros of the Tchebyshev polynomials of second kind:

$$\xi_i = \frac{1}{2}\left(1 - \cos\left[\pi \cdot \frac{i}{I+1}\right]\right) \quad 0 \leqslant i \leqslant I+1.$$

4.5. Adaptive time step control and detection of pseudo steady states

In general, at the beginning of a simulation run, changes in the solution are much larger than at later stages. Therefore, an adaptive time step control technique based on the approach of Johnson et al. [18] has been implemented. As a result, the time step size will be kept smaller as long as one observes high gradients, generally at the beginning of the simulation. Time step sizes are much larger when the solution is close to equilibrium. As a result, the control of the time step size can guarantee fast simulations preserving good accuracy and avoiding high computational cost. The stability of the fully implicit approach allows to control the size of the time steps without taking into account possible stability constraints.

The time integration procedure is described as follows. First, sampling times $T^0, T^1, \ldots, T^N$ subdividing the time interval $[T^0, T^N]$ are defined. The computation of the solution is enforced at these times, which makes possible comparisons between the adaptive time step size method with different control parameters and the approach using a constant time step without the need to interpolate solutions. In practice, coarser sampling intervals are considered at the end of the simulation when the solution is expected to become smoother. At the beginning, these intervals are arranged in a finer way. Then, the time discretization $T^j + t^{j,k}$ within each sampling interval $[T^j, T^{j+1}]$ is carried out by the following adaptive method:

(i) Given an initial solution Z^0, a solution $Z^{j,k}$ is computed on each sampling interval $[T^j, T^{j+1}]$ at each time step $T^j + t^{j,k}$, for $T^j \leqslant T^N$.
(ii) At each time step, Newton's method is used to solve the system $F(Z) = 0$.
(iii) The time integration involves a control of the time step size based on the difference between two successive time iterates $\|Z^{j,k+1} - Z^{j,k}\|$. For that purpose, a tolerance δ is introduced, which ensures the appropriate variation of the time step size:

$$\mathcal{E}_\sigma^{j,k} = \|Z_\sigma^{j,k+1} - Z_\sigma^{j,k}\| \leqslant \mathcal{W}_\sigma \delta, \quad \sigma \in \Sigma = \{\Psi, P, N, C, V, X_0, X_1\}. \tag{4.9}$$

Here, $\mathcal{W} = \{\mathcal{W}_\sigma\}_{\sigma\in\Sigma}$ is a vector of weights related to the different physical variables, and Z_σ is the part of Z which relates to the physical variable $\sigma \in \Sigma$. The weights are adjusted considering the errors between two successive time iterates at the beginning of simulation.

(iv) If the error $\mathcal{E}^{j,k} = \max_{\sigma\in\Sigma}\mathcal{E}_\sigma^{j,k}$ is not small enough, the time step size is divided by 2 and the next iterate $Z^{j,k+1}$ at time $T^j + t^{j,k} + \Delta t^{j,k+1}$ is computed again. If not, the next iterate is accepted and the next time step size is updated:

$$\Delta t^{j,k+2} = \min_{\sigma\in\Sigma} \frac{\Delta t^{j,k+1}\ \mathcal{W}_\sigma\ \delta}{\|Z_\sigma^{j,k+1} - Z_\sigma^{j,k}\|}.$$

Please cite this article in press as: C. Bataillon et al., Numerical methods for the simulation of a corrosion model with moving oxide layer, J. Comput. Phys. (2012), http://dx.doi.org/10.1016/j.jcp.2012.06.005

(v) We choose an appropriate minimum time step size Δt_{min}, which ensures bounded relative error $\mathcal{E}^{J,k}, J \leqslant J_0, k \leqslant k_0$ during the first J_0, k_0 time steps. Then we enable the time step size control by Eq. (4.9) from the $J_0, k_0 + 1$ time steps.

The outline of the algorithm for adaptive time step control is given as follows:

(1) Compute the initial data Z^0
(2) $\Delta t^{0,1} = \Delta t_{min}$
(3) For $J = 0$ to N
(3.1) For each time step $T^J + t^{J,k} \leqslant T^{J+1}$
(3.1.a) Perform Newton's method to compute the new iterate $Z^{J,k+1}$ by solving $F(Z^{J,k+1}) = 0$
(3.1.b) If $\|Z_\sigma^{J,k+1} - Z_\sigma^{J,k}\| \leqslant \mathcal{W}_\sigma\ \delta,\ \forall \sigma \in \Sigma$
Then accept $Z^{J,k+1}$, and choose

$$\Delta t^{J,k+2} = \min_{\sigma \in \Sigma} \frac{\Delta t^{J,k+1} \mathcal{W}_\sigma\ \delta}{\|Z_\sigma^{J,k+1} - Z_\sigma^{J,k}\|}$$

else $\Delta t^{J,k+1} = \Delta t^{J,k+1}/2$ and go to (3.1.a)

Of particular interest are pseudo steady states of the system which are characterized by the equilibrium between the rates of oxide layer creation at the metallic interface and oxide layer dissolution at the solute interface. As a consequence, one would observe a moving oxide layer of constant thickness. In terms of the transformed system (3.2)–(3.4) such states are characterized by the stationarity of the unknowns Ψ, N, P, C and the oxide layer thickness L, while the boundary positions $X_0(t), X_1(t)$ are still evolving.

Therefore, we assume that the system has reached a pseudo steady state and terminate the simulation if the change in the thickness of the oxide layer is small compared to the velocity of the metallic interface:

$$\frac{\left|\left(X_1^{J,k+1} - X_1^{J,k}\right) - \left(X_0^{J,k+1} - X_0^{J,k}\right)\right|}{\left|X_1^{J,k+1} - X_1^{J,k}\right|} < \epsilon.$$

5. Performance of the numerical methods

5.1. Comparison of the different numerical strategies

In this section, we compare the following strategies presented in Section 4:

- Explicit handling of the boundary positions: $\left(\mathcal{S}_{tot}^{e}\right)$. For the galvanostatic case, we use a fixed point method to calculate the corrosion potential.
- Implicit handling of the boundary positions: $\left(\mathcal{S}_{tot}^{i}\right)$ and $\left(\mathcal{S}_{tot}^{i,gc}\right)$. In the galvanostatic case, the equation for V is added in the nonlinear system of equations. We will compare the results obtained with a fixed time step and with the adaptive time step strategy.

The results in this section have been obtained using a model without the boundary velocity terms in (1.1b), (1.1c), (1.2b), (1.2c), (1.3b), (1.3c). No significant difference to the numerical performance of the full model has been observed.

Table 5.1 presents for all cases the total number of Newton iterations required during a given simulation and the corresponding CPU time. For the adaptive time step approach, the parameter δ has been fixed to $\delta = 0.1$ and the weights $\mathcal{W}$ are:

$$\left(\mathcal{W}_\Psi = 0.05,\ \mathcal{W}_P = 0.05,\ \mathcal{W}_N = 0.05,\ \mathcal{W}_C = 0.1, \mathcal{W}_V = 0.05,\ \mathcal{W}_{X_0} = 0.5,\ \mathcal{W}_{X_1} = 0.01\right).$$

Table 5.1
Comparison of the performance of the different solution strategies.

	Potentiostatic case (T_{max} = 601 h)		Galvanostatic case (T_{max} = 219 h)	
	CPU time (s)	Newton its.	CPU time (s)	Newton its.
$\left(\mathcal{S}_{tot}^{e}\right)$, $\Delta t = 5 \cdot 10^{-3}$ h	$8.71 \cdot 10^3$	221,793	$4.97 \cdot 10^4$	1,316,084
$\left(\mathcal{S}_{tot}^{i}\right)$ fixed $\Delta t = 5 \cdot 10^{-3}$ h	$1.49 \cdot 10^4$	240,526	$3.72 \cdot 10^3$	111,472
$\left(\mathcal{S}_{tot}^{i}\right)$ adaptive time step ($\Delta t_{min} = 5 \cdot 10^{-3}$ h)	$2.48 \cdot 10^2$	4027	$3.79 \cdot 10^2$	6233

Please cite this article in press as: C. Bataillon et al., Numerical methods for the simulation of a corrosion model with moving oxide layer, J. Comput. Phys. (2012), http://dx.doi.org/10.1016/j.jcp.2012.06.005

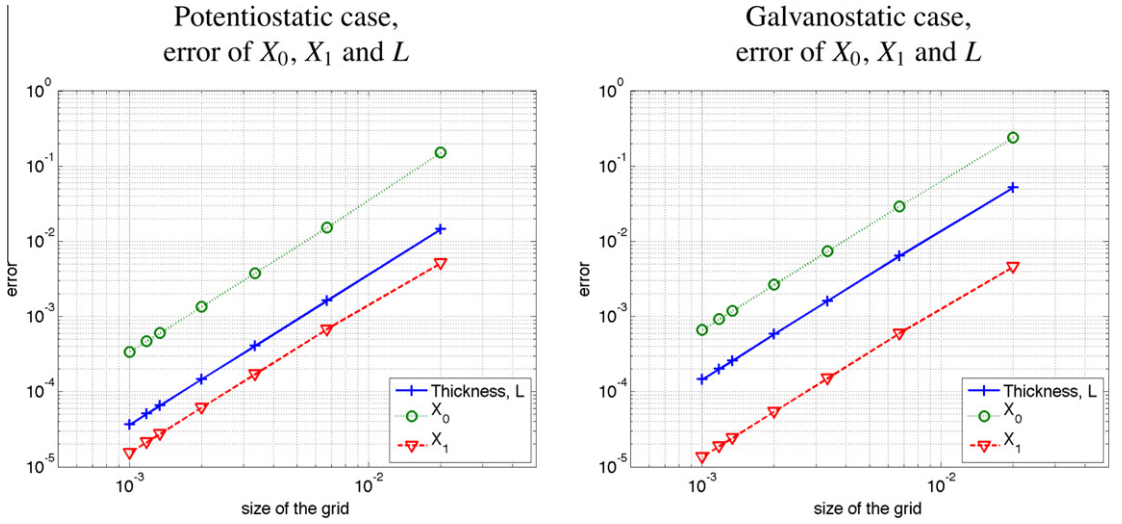

Fig. 5.1. Estimated error: difference between the boundary positions for different grid sizes and a those of a reference solution computed on a grid with 30,000 points after 2 h, for $\delta = 0.1$ and $\Delta t_{min} = 5 \cdot 10^{-3}$ h.

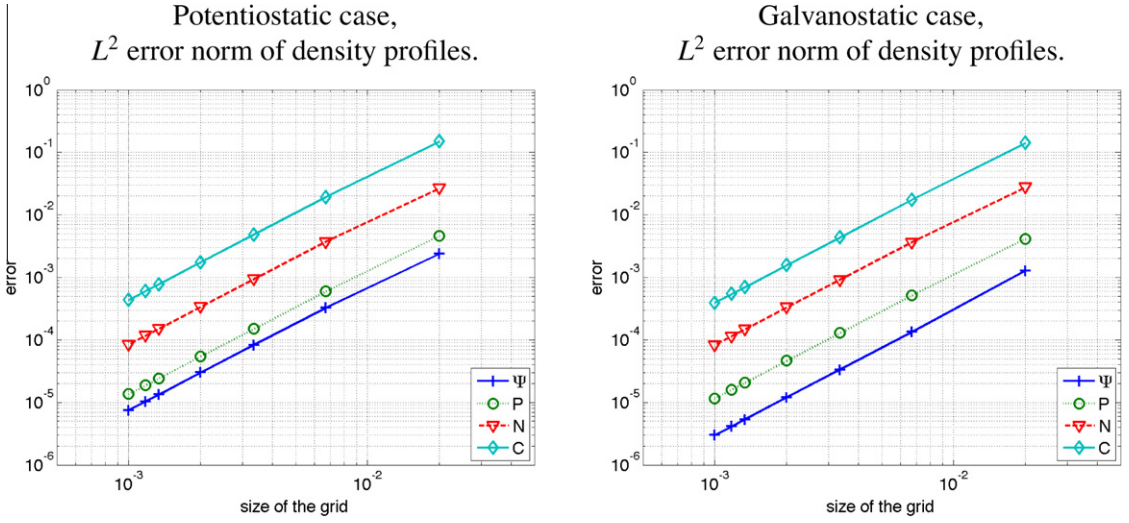

Fig. 5.2. Estimated error: difference between the discrete solutions for different grid sizes and a reference solution computed on a grid with 30,000 points after 2 h, for $\delta = 0.1$ and $\Delta t_{min} = 5 \cdot 10^{-3}$ h.

We note that the use of a constant time step enforces the algorithm to proceed over the full simulation interval with the small time step required by the first time iteration. The use of the adaptive time step approach together with implicit handling of the boundary positions provides satisfactory times of computation.

5.2. Order of convergence in space and time

Since no exact solution is available for this problem, we estimate the error by calculating the difference to a reference solution computed on a fine space-and-time grid.

Figs. 5.1 and 5.2 respectively report the error for the interface positions and the density profiles for the schemes $\left(\mathcal{S}^{i}_{tot}\right)$ and $\left(\mathcal{S}^{i,gc}_{tot}\right)$ (see Sections 4.2 and 4.3). Grid sizes range from $h = 10^{-3}$ to $h = 2 \times 10^{-2}$, and the time step was chosen adaptively. For all the plotted quantities, the second order convergence in space is confirmed. Such order can be expected due to the choice of the Bernoulli function in the definition of the numerical fluxes, as it has been proven for model problems in [14,15].

In order to check the convergence in time of our method, we have run simulations with some fixed time steps and compare the obtained solutions to a reference solution computed with a small time step. Fig. 5.3 demonstrates the first order

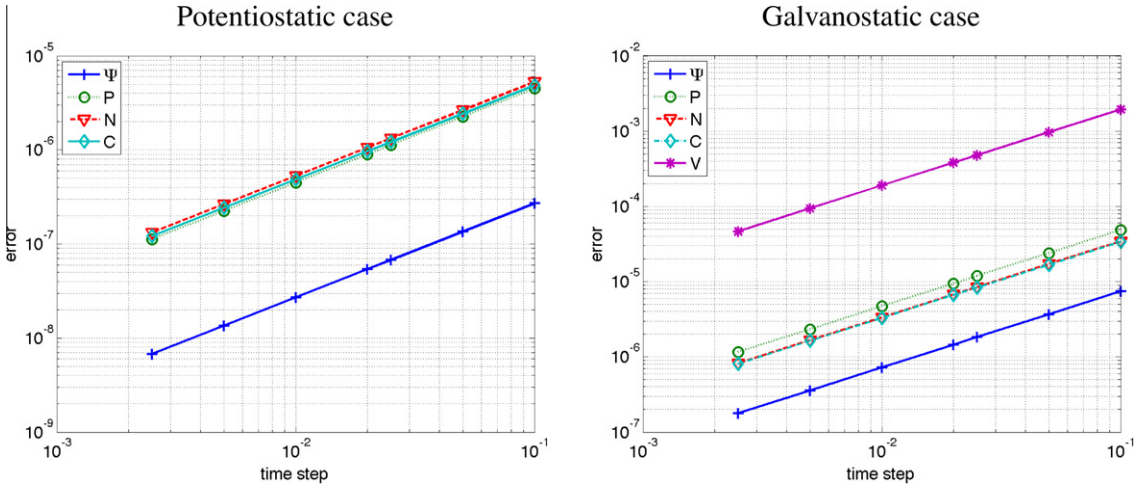

Fig. 5.3. Estimated error: difference after 2 h between discrete solutions with 2000 grid points for different values of a fixed time step Δt and a reference solution computed with $\Delta t = 2 \cdot 10^{-6}$ h.

Table 5.2
Average number of Newton steps per time step.

Potentiostatic case (T_{max} = 601 h)			Galvanostatic case (T_{max} = 219 h)		
Time steps	Newton steps	Average	Time steps	Newton steps	Average
1453	4027	2.77	1740	6233	3.58

convergence in time for the density profiles and the free corrosion potential (in the galvanostatic case). Similar results are obtained for the interface positions.

5.3. Newton convergence

Concerning the convergence rate of Newton's method, Table 5.2 shows that the average number of Newton steps per time step is small. The main deviation from this average number happens during the first time step. In general, we observe quadratic convergence of Newton's method.

6. Numerical experiments

The physico-chemical parameters for claystones chosen are based on the values found in the literature [19], where potentiostatic measurements have been reported for the potential range from −0.15 to 1.05 V/NHE. Their results have been obtained using a borate buffer solution which allows for an experimental environment with controlled pH value, whereas the buffer system itself is inert with respect to the process under investigation. In a similar context, a borate buffer solution has been used in [20].

The other parameters of the DPCM, which describe the metal and oxide layer characteristics, the kinetics and the electrostatic potential are discussed in Ref. [1].

Some of them can be found in the literature [21–29]. Table 6.1 gives the values.

6.1. Potentiostatic case

Fig. 6.1(a) shows the current density after reaching constant thickness, i.e., constant and equal interface velocities. For the three pH values, the current density becomes potential independent at less negative potentials. This corresponds to the well-known passive current density [30]. It must be outlined that the passive current decreases with pH. Such behavior is well documented in the literature [31]. For the same data, Fig. 6.1(b) plots the dependency of the oxide layer thickness on the applied potential. The constant thickness reaches zero at certain value of the potential called passivation potential E_p [30]. For values of the applied potential less than E_p, the surface of the metal is not covered by any oxide layer. From the figure, we can read the passivation potentials $E_p = -0.45$ V/NHE at pH 7, $E_p = -0.6$ V/NHE at pH 8, and $E_p = -0.64$ V/NHE at pH 9.

Please cite this article in press as: C. Bataillon et al., Numerical methods for the simulation of a corrosion model with moving oxide layer, J. Comput. Phys. (2012), http://dx.doi.org/10.1016/j.jcp.2012.06.005

Table 6.1
Physical parameters of the test problem.

T (K)	pH	E_{redox} (V/NHE)	$\mathbf{a}_{Fe^{+2}}$ (mol · m^{-3})
298	7	−0.2	$1 \cdot 10^{-8}$
$\mathbf{a}_{Fe^{+3}}$ (mol · m^{-3})	R (j · k^{-1} · mol^{-1})	k (J · K^{-1})	F (C · mol^{-1})
$2.7496 \cdot 10^{-25}$	8.32	$1.38 \cdot 10^{-23}$	$9.6487 \cdot 10^{4}$
χ_0 (F · m^{-2})	m_e (kg)	Ω_{Fe} (m^3 · mol^{-1})	n_{DOS} (mol · (m^{-3} · J^{-1}))
$8.854 \cdot 10^{-12}$	$9.11 \cdot 10^{-31}$	$7.105 \cdot 10^{-6}$	$1.35 \cdot 10^{24}$
L_0 (m)	Ω_{ox} (m^3 · mol^{-1})	χ	D_1 (m^2 · s^{-1})
$3 \cdot 10^{-9}$	$4.474 \cdot 10^{-5}$	10	$1 \cdot 10^{-20}$
D_2 (m^2 · s^{-1})	D_3 (m^2 · s^{-1})	Γ_0 (F · m^{-2})	Γ_1 (F · m^{-2})
$1 \cdot 10^{-6}$	$1 \cdot 10^{-20}$	0.5	1
$\Delta\Psi_0^{pzc}(V)$	$\Delta\Psi_1^{pzc}(V)$	V (V/ENH)	k_{Fe}^0 (m · s^{-1})
0.392–0.059 pH	0	$V_{imposed}$	50
m_{Fe}^0 (m · s^{-1})	k_{Fe}^1 (m · s^{-1})	m_{Fe}^1 (m · s^{-1})	k_e^0 (m · s^{-1})
6.65203	1	0.1	$1 \cdot 10^{-8}$
m_e^0 (mol · (m^{-2} · s^{-1}))	k_r^0 (m · s^{-1})	m_r^0 (mol · (m^{-2} · s^{-1}))	k_{ox}^0 (mol · (m^{-2} · s^{-1}))
$3.80943 \cdot 10^{-5}$	3.67525	$1 \cdot 10^{-9}$	$1 \cdot 10^{41}$
m_{ox}^0 (mol · (m^{-2} · s^{-1}))	k_{ox}^1 (mol · (m^{-2} · s^{-1}))	m_{red}^1 (mol · (m^{-2} · s^{-1}))	k_d^0 (pH) (mol · (m^{-2} · s^{-1}))
10	$1 \cdot 10^{-6}$	$1 \cdot 10^{-5}$	$0.2 \cdot 10^{-\mathrm{pH}}$
$\left(a_u^0, b_u^0\right)$ $(u = P,N,C,r)$	$\left(a_u^1, b_u^1\right)$ $(u = P,C)$	a_d^0	
(0.5, 0.5)	(0.5, 0.5)	0	

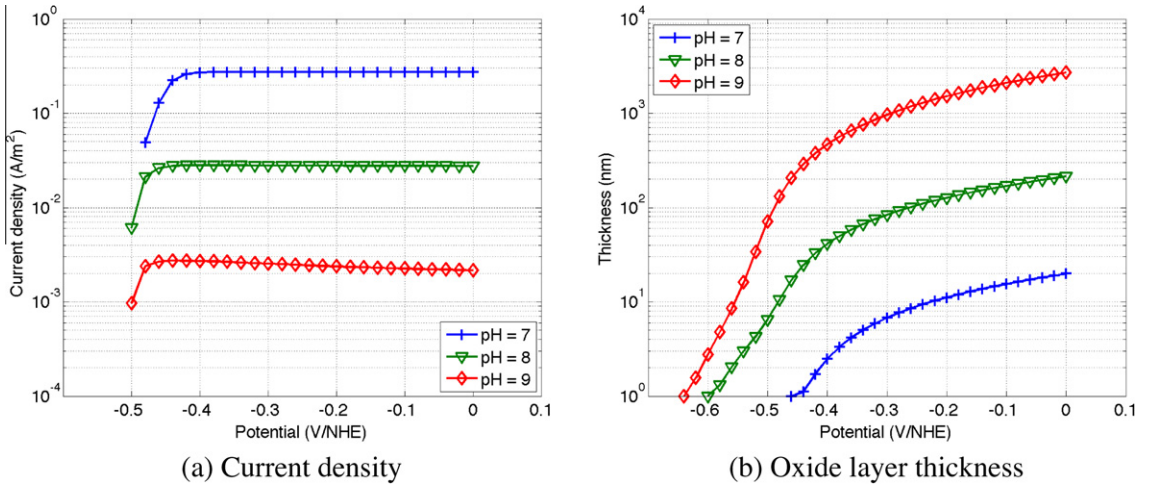

Fig. 6.1. Current density and oxide layer thickness after reaching pseudo steady state vs. applied potential, for different pH values in claystones. Parameter values are given in Table 6.1.

6.2. Galvanostatic case

The left plot in Fig. 6.2 shows the dependency of the thickness of the oxide layer on the pH value. The so-called steady state thickness follows a logarithmic law with a slope equal to 1. This behavior is directly linked to the chosen pH dependency $k_d^0 = 0.2 \cdot 10^{-\mathrm{pH}}$. The thickness reaches zero at the passivation pH value which is 7.2 for the data used. This feature of the passivity is similar to the passivation potential E_p but for spontaneous passivation. The value predicted is in accordance with the literature [32]. Please note that the time to reach a constant interface velocity (pseudo steady state) strongly depends on the pH value, and may reach thousands of years in concrete. From an experimental point of view, the pseudo steady state is considered as reached when the thickness does not evolve significantly over several hours. This explains why the experimental curves published in the literature correspond to the curve obtained for 1 month. The break of the slope has been attributed to a change in the dissolution mechanism. The results presented here indicate that the break of the slope results mainly from the fact that the experimental time was too short to reach an actual pseudo steady state.

Please cite this article in press as: C. Bataillon et al., Numerical methods for the simulation of a corrosion model with moving oxide layer, J. Comput. Phys. (2012), http://dx.doi.org/10.1016/j.jcp.2012.06.005

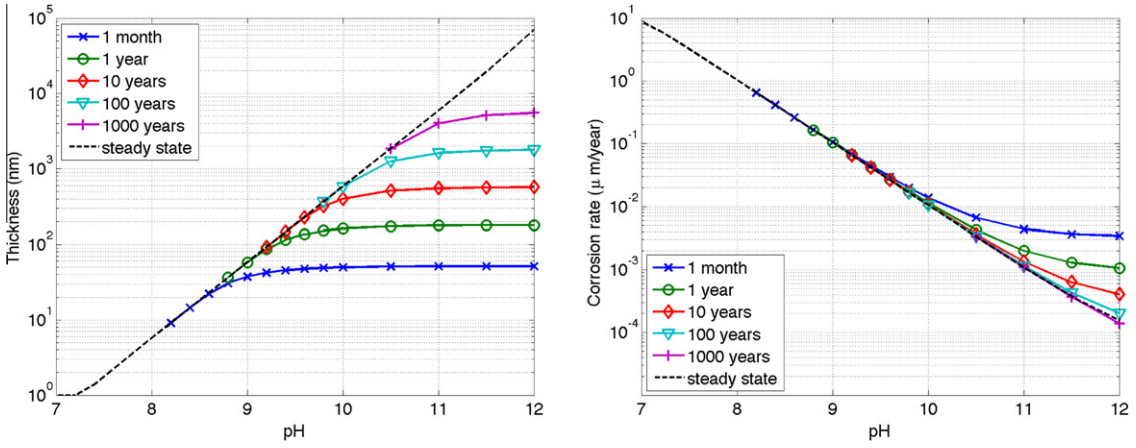

Fig. 6.2. Thickness of the oxide layer (left) and corrosion rate (right) depending on pH value.

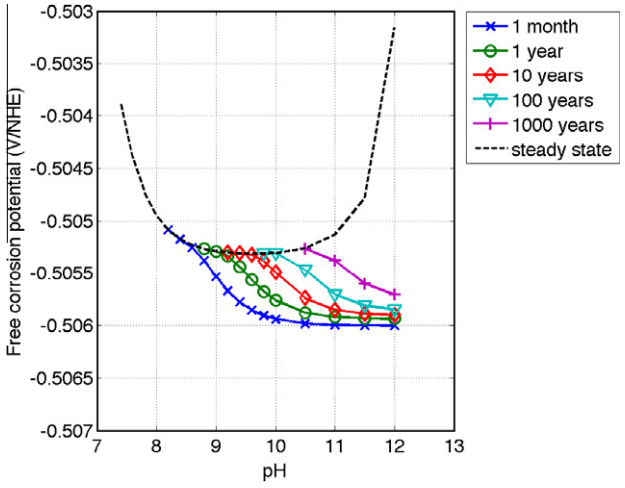

Fig. 6.3. Free corrosion potential vs. pH value.

The right plot in Fig. 6.2 shows the evolution of the corrosion rate with respect to the pH value. The pseudo steady state corrosion rate decreases with the pH value with an order equal to -1 (linear in log plot). This was an expected result because in anaerobic condition the oxidant is water or more precisely the proton [30]. As the proton activity in the solution has been defined as 10^{-pH}, the decrease shown in the right plot in Fig. 6.2 simply depicts that in pseudo steady state, the corrosion rate is directly proportional to the activity of protons in solution.

In order to perform the calculations corresponding to Figs. 6.2 and 6.3, the number of nodes in the discretization grid has been significantly increased in order to accommodate the comparably thick oxide layers in the case of high pH values. As a consequence, the computation time to obtain these results was 32.9 h (for the full range of pH values). Fine tuning of the numerical parameters may allow to reduce this number if necessary.

6.3. Further remarks

The numerical experiments in both cases (potentiostatic and galvanostatic) suggest the existence of a pseudo steady state which is characterized by a constant thickness of the oxide layer and a constant velocity of the interface. The time to reach this steady state strongly depends on the pH value of the surrounding media. Future work will focus on the mathematical analysis of this steady state.

While the presented data show that the model delivers meaningful results, we need to note that several parameters of the model, in particular the Butler Volmer coefficient a_d^0, are subject to discussion in the literature.

While verification of the model by comparison to analytical results has been performed [1], future work among other topics will focus on comparison to experimental results with the potential to support the identification of currently uncertain

Please cite this article in press as: C. Bataillon et al., Numerical methods for the simulation of a corrosion model with moving oxide layer, J. Comput. Phys. (2012), http://dx.doi.org/10.1016/j.jcp.2012.06.005

parameters of the model. In particular, it appears to be possible to incorporate the numerical model into a numerical procedure for parameter identification.

Another focus of future activities is the coupling of the present model to a geochemical model of the surroundings including the investigation of the role of the porous hydroxide layer.

References

[1] C. Bataillon, F. Bouchon, C. Chainais-Hillairet, C. Desgranges, E. Hoarau, F. Martin, S. Perrin, M. Turpin, J. Talandier, Corrosion modelling of iron based alloy in nuclear waste repository, Electrochim. Acta 55 (15) (2010) 4451–4467.
[2] M.E. Gurtin, Thermomechanics of Evolving Phase Boundaries in the Plane, Oxford University Press, 1993.
[3] A. Muntean, M. Böhm, A moving-boundary problem for concrete carbonation: global existence and uniqueness of weak solutions, J. Math. Anal. Appl. 350 (1) (2009) 234–251.
[4] H. Gajewski, On existence, uniqueness and asymptotic behavior of solutions of the basic equations for carrier transport in semiconductors, ZAMM 65 (2) (1985) 101–108.
[5] H. Gajewski, On the uniqueness of solutions to the drift–diffusion model of semiconductor devices, Math. Models Methods Appl. Sci. 4 (1) (1994) 121–133.
[6] W. Fang, K. Ito, On the time-dependent drift–diffusion model for semiconductors, J. Diff. Eq. 117 (2) (1995) 245–280.
[7] W. Fang, K. Ito, Global solutions of the time-dependent drift–diffusion semiconductor equations, J. Diff. Eq. 123 (2) (1995) 523–566.
[8] W. Fang, K. Ito, Asymptotic behavior of the drift–diffusion semiconductor equations, J. Diff. Eq. 123 (2) (1995) 567–587.
[9] H. Gajewski, K. Gröger, Reaction–diffusion processes of electrically charged species, Math. Nachr. 177 (1) (1996) 109–130.
[10] T. Aiki, A. Muntean, Existence and uniqueness of solutions to a mathematical model predicting service life of concrete structures, Adv. Math. Sci. Appl. 19 (1) (2009) 109–129.
[11] T. Aiki, A. Muntean, Large time behavior of solutions to a moving-interface problem modeling concrete carbonation, Commun. Pure Appl. Anal. 9 (5) (2010) 1117.
[12] T. Aiki, A. Muntean, On uniqueness of a weak solution of one-dimensional concrete carbonation problem, Discrete Contin. Dyn. Syst. 29 (4) (2011) 1345–1365.
[13] C. Chainais-Hillairet, J. Droniou, Finite-volume schemes for noncoercive elliptic problems with Neumann boundary conditions, IMA J. Numer. Anal. 31 (1) (2011) 61–85.
[14] A.M. Il'in, A difference scheme for a differential equation with a small parameter multiplying the second derivative, Mat. Zametki 6 (1969) 237–248.
[15] R.D. Lazarov, I.D. Mishev, P.S. Vassilevski, Finite volume methods for convection–diffusion problems, SIAM J. Numer. Anal. 33 (1) (1996) 31–55.
[16] A. Prohl, M. Schmuck, Convergent discretizations for the Nernst–Planck–Poisson system, Numer. Math. 111 (4) (2009) 591–630.
[17] A. Glitzky, K. Gärtner, Energy estimates for continuous and discretized electro-reaction–diffusion systems, Nonlinear Anal. 70 (2) (2009) 788–805.
[18] C. Johnson, Y.-Y. Nie, V. Thomée, An a posteriori error estimate and adaptive timestep control for a backward euler discretization of a parabolic problem, SIAM J. Numer. Anal. 27 (2) (1990) 277–291.
[19] Z. Szklarska-Smialowska, W. Kozlowski, Electrochemical and ellipsometric investigations of passive films formed on iron in borate solutions, J. Electrochem. Soc. 131 (2) (1984) 234–241.
[20] J. Trefz, M. Schweinsberg, T. Reier, J.W. Schultze, Systematic investigation on the corrosion of iron under conditions relevant to storage of nuclear waste, Mater. Corros. 47 (9) (1996) 475–485.
[21] M.I. Klinger, A.A. Samokhvalov, Electron conduction in magnetite and ferrites, Phys. Stat. Sol. 79 (1) (1977) 9–48.
[22] M. Backhaus-Ricoult, R. Dieckmann, Defects and cation diffusion in magnetite (vii): diffusion controlled formation of magnetite during reactions in the iron–oxygen system, Ber. Bunsenges. Phys. Chem. 90 (8) (1986) 690–698.
[23] J.E. Parrott, Reformulation of boundary conditions at metal–semiconductor contacts, in: Metal–semiconductor Contacts, Manchester Conference Series, vol. 22, Institute of Physics, London, 1974, p. 20.
[24] V.L. Moruzzi, J.F. Janak, A.R. Williams, Calculated Electronic Properties of Metals, Pergamon Press, 1978.
[25] M. Büchler, P. Schmuki, H. Böhni, Iron passivity in borate buffer, J. Electrochem. Soc. 145 (2) (1998) 609–614.
[26] P.A. Castro, E.R. Vago, E.J. Calvo, Surface electrochemical transformations on spinel iron oxide electrodes in aqueous solutions, J. Chem. Soc. Faraday Trans. 92 (18) (1996) 3371–3379.
[27] E. Sikora, D.D. MacDonald, The passivity of iron in the presence of ethylenediaminetetraacetic acid. I. General electrochemical behavior, J. Electrochem. Soc. 147 (11) (2000) 4087–4092.
[28] L. Garcell, M.P. Morales, M. Andres-Verges, P. Tartaj, C.J. Serna, Interfacial and rheological characteristics of maghemite aqueous suspensions, J. Colloid Interface Sci. 205 (2) (1998) 470–475.
[29] R.E. Hummel, Electronic Properties of Materials, Springer, 1985.
[30] D. Landolt, Corrosion and Surface Chemistry of Metals, EFPL Press, 2007.
[31] N. Sato, T. Noda, Ion migration in anodic barrier oxide films on iron in acidic phosphate solutions, Electrochim. Acta 22 (8) (1997) 839–843.
[32] M.A. Climent, C. Gutierrez, Proof by UV–visible modulated reflectance spectroscopy of the breakdown by carbonation of the passivating layer on iron in alkaline solution, Surface Sci. 330 (1) (1995) 651–656.

Please cite this article in press as: C. Bataillon et al., Numerical methods for the simulation of a corrosion model with moving oxide layer, J. Comput. Phys. (2012), http://dx.doi.org/10.1016/j.jcp.2012.06.005